Title

Calcium dysregulation and Cdk5-ATM pathway involved in a mouse model of fragile X-associated tremor/ataxia syndrome

Journal

Human Molecular Genetics, 26(14)

ISSN

0964-6906

Authors

Robin, Gaëlle

López, José R

Espinal, Glenda M

et al.

Publication Date

2017-07-15

DOI

10.1093/hmg/ddx148

Peer reviewed

Human Molecular Genetics, 2017, Vol. 26, No. 14 2649–2666

doi: 10.1093/hmg/ddx148
Advance Access Publication Date: 21 April 2017
Original Article

ORIGINAL ARTICLE

Calcium dysregulation and Cdk5-ATM pathway involved in a mouse model of fragile X-associated tremor/ataxia syndrome

Gaëlle Robin[1], José R. López[1], Glenda M. Espinal[2], Susan Hulsizer[1], Paul J. Hagerman[2,3] and Isaac N. Pessah[1,3,*]

[1]Department Molecular Biosciences, School of Veterinary Medicine, Davis, CA, USA, [2]Department of Biochemistry and Molecular Medicine, UC Davis, Davis, CA 95616, USA and [3]Medical Investigations of Neurodevelopmental Disorders (MIND) Institute, Sacramento, CA 95817, USA

*To whom correspondence should be addressed at: Department of Molecular Biosciences, UC Davis, 1089 Veterinary Medicine Way, 1020 VM3B, Davis, CA 95616, USA. Tel: +1 530 7526696; Fax: +15307527690; Email: inpessah@ucdavis.edu

Abstract

Fragile X-associated tremor/ataxia syndrome (FXTAS) is a neurological disorder that affects premutation carriers with 55-200 CGG-expansion repeats (preCGG) in *FMR1*, presenting with early alterations in neuronal network formation and function that precede neurodegeneration. Whether intranuclear inclusions containing DNA damage response (DDR) proteins are causally linked to abnormal synaptic function, neuronal growth and survival are unknown. In a mouse that harbors a premutation CGG expansion (preCGG), cortical and hippocampal FMRP expression is moderately reduced from birth through adulthood, with greater FMRP reductions in the soma than in the neurite, despite several-fold elevation of *Fmr1* mRNA levels. Resting cytoplasmic calcium concentration ($[Ca^{2+}]_i$) in cultured preCGG hippocampal neurons is chronically elevated, 3-fold compared to Wt; elevated ROS and abnormal glutamatergic responses are detected at 14 DIV. Elevated μ-calpain activity and a higher p25/p35 ratio in the cortex of preCGG young adult mice indicate abnormal Cdk5 regulation. In support, the Cdk5 substrate, ATM, is upregulated by 1.5- to 2-fold at P_0 and 6 months in preCGG brain, as is p-Ser^{1981}-ATM. Bax:Bcl-2 is 30% higher in preCGG brain, indicating a greater vulnerability to apoptotic activation. Elevated $[Ca^{2+}]_i$, ROS, and DDR signals are normalized with dantrolene. Chronic $[Ca^{2+}]_i$ dysregulation amplifies Cdk5-ATM signaling, possibly linking impaired glutamatergic signaling and DDR to neurodegeneration in preCGG brain.

Introduction

Fragile X-associated tremor/ataxia syndrome (FXTAS), initially described as a late-onset disorder, is a neurodegenerative disease that affects carriers of the premutation CGG-repeat allele (preCGG; 55-200 repeats) of the fragile X mental retardation 1 (*FMR1*) gene (1). Larger expansions (>200 repeats; full mutation) result in hypermethylation of the *FMR1* gene in humans and subsequent transcriptional silencing. The consequent absence of the *FMR1* protein (FMRP) leads to the fragile X syndrome (FXS), the most common inherited form of cognitive disability and syndromic autism (2). Premutation alleles have estimated frequencies of 1 in 250–810 males and 1 in 130–250 females (3,4), and carriers can present a range of clinical features that include primary ovarian insufficiency (20%) and, later in life, FXTAS in males and females (40% and 20%, respectively) above 50 years (5). FXTAS is characterized clinically by intention tremor, gait ataxia, dementia, and peripheral neuropathy, and neuropathologically by single inclusions in some of the nuclei

Received: February 28, 2017. **Revised:** April 6, 2017. **Accepted:** April 12, 2017

of the brain and brain tissue loss (6). Although FXTAS is diagnosed as a late-adult-onset disorder, recent studies in young premutation carriers demonstrated higher rates of autism and attention deficit hyperactivity disorder in the absence of any features of FXTAS, suggesting that the *FMR1* premutation affects brain function much earlier in life (6–8). Indeed, premutation alleles of the *FMR1* gene are associated with defects in developmental programs operating during the prenatal stage of the brain formation of *FMR1* premutation knock-in mice (preCGG KI) (9). Moreover, abnormal neurite outgrowth and synaptic architecture have been shown in hippocampal neurons from preCGG KI as early as 7 days *in vitro* (DIV) (10), an *in vitro* finding that recapitulates morphometric analyses in preCGG KI brain (11,12). In addition, early abnormal Ca^{2+} dynamics associated with impaired mGluR1/5 signaling have been identified in neuronal and astrocytic cells from preCGG KI mice (13–15), as well as in older human premutation carriers with FXTAS (16) and in induced pluripotent stem cell (iPSC)-derived neurons prepared from a human premutation carrier (17).

Mouse and human premutation carriers display gene dysregulation with increased levels of *FMR1* mRNA and decreased FMRP expression (11,18), suggesting that the disease is caused by excess CGG-repeat-containing *FMR1* mRNA (19–21). Consistent with this mRNA toxicity hypothesis, intranuclear inclusions found in neuronal and glial cells of FXTAS patients (22,23) and preCGG KI mice (19) contain both *FMR1* mRNA (24) and proteins of the DNA damage response (DDR) (22,24–27). Recently, an alternative mechanism, repeat associated non-AUG translation (RAN), has been proposed to play a role in inclusion formation and cytotoxicity (28–31). The large number of CGG repeats in the DNA can trigger RAN translation to produce a potentially toxic protein, FMRpolyG, which is thought to accumulate in both cellular- and mouse-based disease models. FMRpolyG has also been detected in ubiquitinated neuronal intranuclear inclusions of FXTAS patients (28,31).

The links between the early-onset abnormalities in neuronal morphology and synaptic activity and the late-onset mechanisms leading to FXTAS are unknown. Based on our observations suggesting involvement of DDR in FXTAS pathogenesis, we hypothesize a role for two key signaling kinases, ataxia telangiectasia mutated (ATM) and cyclin-dependent kinase 5 (Cdk5), to be involved in both synaptic signaling and DNA damage repair. Cdk5, a small Ser/Thr kinase regulated by the activator p35, is critical for brain development and neuronal function, including neuronal migration, synaptic transmission, and plasticity (32). Moreover, its subcellular localization and kinase activity are tightly regulated by Ca^{2+} dynamics triggered by neuronal activity, primarily through calpain-dependent cleavage of Cdk5/p35 to Cdk5/p25 in the cytoplasm (33). Redistribution of Cdk5/p25 to the nucleus can directly phosphorylate ATM, a phosphatidylinositol-3-kinase-like kinase, at Ser 784, required for auto-phosphorylation at Ser1981 (p-Ser^{1981}-ATM) (34–36). Activation of nuclear ATM represents an early response to double-stranded DNA breaks that initiates DDR and regulates the balance between cell survival and apoptosis (37). p-Ser^{1981}-ATM is also a cytoplasmic signaling mediator, phosphorylating hundreds of protein substrates that activate and coordinate cell-cycle checkpoints, nuclear localization, gene transcription, and responses to ROS (38,39).

To assess the involvement of Cdk5 and ATM in the early events of FXTAS pathogenesis, we investigated brains and primary cultured neurons isolated from preCGG KI mice (11). We show that preCGG neurons have early dysregulation of Ca^{2+} homeostasis, resulting in an over-activation of μ-calpain, skewing of p35/p25, and hyperphosphorylation of ATM. Elevated p-Ser^{1981}-ATM in preCGG neurons is associated with enhanced Bax/Bcl2 and higher vulnerability to ROS. Based on the results of this study, we propose that in the presence of *Fmr1* expansion repeats in the premutation range, chronic Ca^{2+} dysregulation amplifies the Cdk5-ATM signaling pathway, with this process beginning early in postnatal development.

Results

FMRP is down-regulated in cortical and hippocampal tissue across postnatal stages

The Rotterdam knock-in preCGG mouse model (150–200 CGG expansion range) (11,19) was used to evaluate possible links among abnormal Ca^{2+} dynamics, Cdk5/ATM signaling, and ROS. Like human premutation patients, the expression of FMRP is modestly to moderately downregulated at P_0 in both cortical ($32.1 \pm 6.2\%$, $P < 0.0001$) and hippocampal ($18.5 \pm 7.6\%$, $P = 0.0004$) tissue in male preCGG compared to *Wt* mice (Fig. 1A and B). By 6 weeks, FMRP expression in preCGG cortical and hippocampal tissues show a protein downregulation of $49.2 \pm 8\%$ ($P = 0.0342$) and $64.5 \pm 9.5\%$ ($P = 0.0257$) compared to respective *Wt* tissues. At 6 months, FMRP in both regions remains downregulated at approximately 50% relative to *Wt* (cortex, $P = 0.0067$; hippocampus, $P = 0.0025$) (Fig. 1A and B). We also measured FMRP expression in hippocampal neurons in culture, finding similar downregulation. Lysates from 7 DIV preCGG hippocampal neuronal culture from male (preCGG M) and female (preCGG F) P_0 pups exhibit reduced FMRP expression compared to *Wt* male and female (*Wt* M and *Wt* F) cultures (preCGG M: $39.1 \pm 8.7\%$, *Wt M*: $100.0 \pm 7.2\%$, $P = 0.0038$; preCGG F: $45.0 \pm 4.7\%$, *Wt F*: $104.1 \pm 3.2\%$, $P = 0.0013$) (Fig. 1C and D). Furthermore, both cortical and hippocampal tissues dissected from brains of preCGG mice show persistent 2- to 4-fold elevation in *Fmr1 m*RNA compared to respective *Wt* as early as P_0 (cortical) and through six months of age (Supplementary Material, Fig. S1), consistent with previous reports (10,14,15). Also, consistent with our previous report (17), FMRP levels are essentially identical for normal-active and premutation-active alleles in iPSC derived neuronal subclones (Supplementary Material, Fig. S2) despite several-fold elevation of *Fmr1* mRNA levels.

FMRP distribution is changed in preCGG hippocampal neurons

FMRP is an RNA binding protein that not only interacts with a range of mRNA targets but also a variety of intracellular protein partners in the nucleus, cytoplasm, and synapse of neurons. To examine the relationship between overall FMRP expression and its sub-cellular distribution, preCGG and *Wt* hippocampal neurons were probed with anti-FMRP antibody and imaged using immunofluorescence microscopy at 7 DIV and 14 DIV. To only score neuronal FMRP, cellular MAP2B staining was used to create a "filter mask", which was applied to quantify neuronal FMRP staining intensity. Thus, the FMRP intensity was measured only within the mask co-localized with MAP2B positive neurons (Fig. 2A). FMRP expression was assessed in somatic (including the nucleus) and dendritic/axonal processes (Fig. 2A and B). Consistent with our western blot data, total FMRP expression was moderately reduced, by $10.2 \pm 1.1\%$ in preCGG M ($P < 0.0001$) and $18.7 \pm 1.6\%$ in preCGG F neurons ($P < 0.05$) at 7 DIV; and later by $9.0 \pm 1.2\%$ in preCGG M ($P < 0.0001$) and $9.0 \pm 3.0\%$ in preCGG F ($P < 0.001$) neurons 14 DIV, respectively

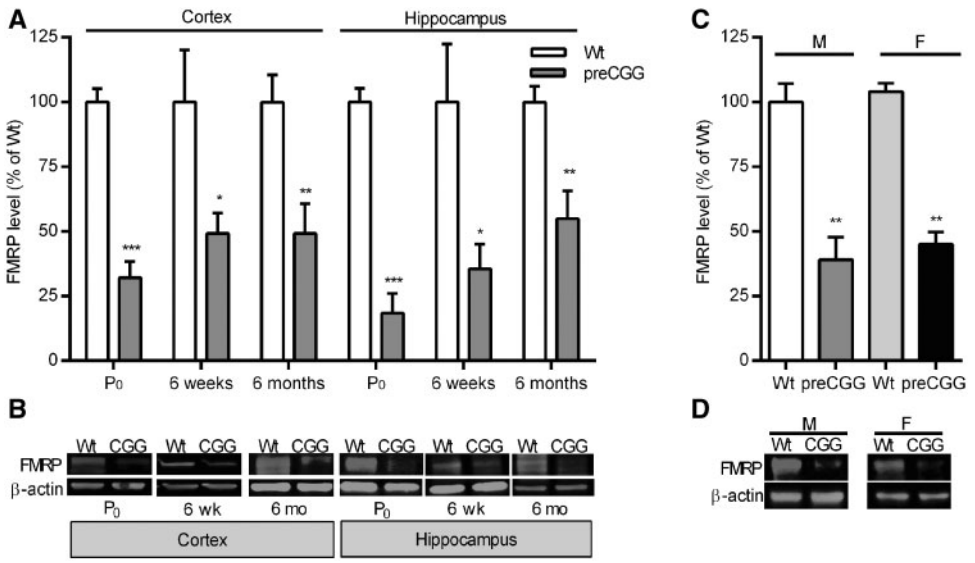

Figure 1. Fragile X mental retardation protein (FMRP) is decreased in preCGG mice across postnatal stages. (**A**) Quantification of FMRP expression level relative to β-actin in cortical and hippocampal tissues from preCGG (Cortex: P_0, $n = 7$; 6 week, $n = 8$; 6 months, $n = 7$. Hippocampus: P_0, $n = 4$; 6 week, $n = 7$; and 6 months, $n = 8$) and age-matched Wt mice (Cortex: P_0&6 week, $n = 8$; 6 months, $n = 7$, Hippocampus: P_0, $n = 3$; 6 weeks and 6 months, $n = 8$), normalized to Wt FMRP expression. (**B**) Representative western blot of FMRP (70kDa) and β-actin (45kDa) from cortical and hippocampal tissues from indicated genotype and age. (**C**) Quantification of FMRP expression levels relative to β-actin in paired Wt ($n = 3$) and preCGG ($n = 4$) male (M) and Wt ($n = 3$) and preCGG ($n = 4$) female (F) cultures of hippocampal neurons at 7 DIV. (**D**) Representative western blot in paired culture of Wt and preCGG hippocampal neurons. Significance was determined using t-test $^*P < 0.05$; $^{**}P < 0.01$; $^{***}P < 0.001$. Error bars indicate mean ± SEM.

compared to Wt. The sub-cellular analysis revealed a surprising finding that, despite the overall decrease in FMRP in preCGG neurons, the FMRP intensities in the neurites were not significantly different between preCCG and Wt; the decrease in FMRP in the somas of preCGG hippocampal neurons was responsible for the bulk of the overall FMRP decrease (Fig. 2B). This result was true at both time points studied and with male and female derived cultures.

Abnormal glutamatergic responses in preCGG hippocampal neurons

Glutamate (Glu) is the most abundant excitatory neurotransmitter in the vertebrate CNS and has been implicated in *FMR1*-related disorders, so we used the intracellular Ca^{2+} response to Glu as a functional assay of 14 DIV hippocampal neurons (40). The Ca^{2+} transient triggered by the addition of 3 μM Glu (Fig. 3A) was longer lasting in preCGG M compared to Wt M (Area under the Curve, 204.8 ± 22.8%, $P < 0.001$; FWHM, 180.8 ± 20.3%, $P < 0.001$) (Fig. 3C and D) without affecting the amplitude of the response (Fig. 3B). Neuronal exposure to Glu induces an increase in the concentration of cytoplasmic Ca^{2+} by directly activating α-amino-3-hydroxy-5-methylisoxazole-4-propionate acid (AMPA) and N-methyl-D-aspartate (NMDA) receptor channels and by indirectly activating voltage-dependent Ca^{2+} channels. Glu also mediates mGluR1/5 signaling by mobilizing Ca^{2+} from Ins(1,4,5)P3-sensitive intracellular Ca^{2+} stores, shown to be dysfunctional in fragile X and other autism spectrum disorders (41). Abnormal mGluR1/5 activities were previously suggested from neuronal cell population measurements in the *FMR1* premutation range (14,16).

Single cell imaging recordings of spontaneous synchronous Ca^{2+} oscillations (SCOs) were made before and after application of the selective mGluR5 agonist DHPG (dihydroxyphenylglycine). Indeed, primary hippocampal neurons of both Wt and preCGG cultures exhibit SCOs, which are physiological signals essential for normal neuronal network development and maturation (42). Spatial and temporal abnormalities in SCO patterns not only impact physiological processes of individual neurons, but also pathophysiological sequelae (43). Figure 3E displays the frequency distribution of the spontaneous synchronous Ca^{2+} oscillation amplitudes of the 4 genotypes at baseline and the frequency distribution 5 min after addition of 50 μM DHPG. Under the basal experimental condition used, neurons cultured separately from male and female mice significantly differ in SCO amplitude distribution for both genotypes (Distribution Wt M vs Wt F: $P < 0.0001$; Distribution preCGG M vs preCGG F: $P < 0.0001$), with female neuronal networks having smaller mean amplitude peaks and a narrower distribution (Fig. 3E). PreCGG M neurons display a SCO distribution significantly different from Wt M, with a wider distribution of SCO amplitudes, including increased incidence of both higher and smaller peak amplitudes compared to Wt M neurons (i.e., width of the distribution (WD) of 0.41 ± 0.04 for Wt M versus 0.8 ± 0.13 for preCGG M; height for Wt M: 14.8 ± 1.1% versus preCGG M: 10.9 ± 0.9%, $P = 0.0022$). In contrast, preCGG F neurons have a baseline SCO amplitude distribution and mean amplitude that are comparable to those of Wt F (WD: 0.2 ± 0.03, height: 22.7 ± 2.3%, for preCGG F; WD: 0.28 ± 0.03 height: 20.1 ± 1.5%, for Wt F) (Fig. 3E).

A sharp contrast between preCGG and Wt neurons was revealed by the mGluR5 agonist. DHPG did not induce any significant changes in the distribution of the SCO amplitude in either preCGG M or preCGG F neurons, whereas in the Wt M and F neurons the distributions shifted to the right and became wider relative to the basal distributions, while the height decreased significantly ($\Delta F/F_0$ value at the center of the distribution, Wt M: 0.56 ± 0.04 versus Wt M + DHPG: 0.93 ± 0.15, Wt F: 0.48 ± 0.02 versus Wt F + DHPG: 0.86 ± 0.043; WD, Wt M + DHPG: 1.2 ± 0.2, Wt F + DHPG: 0.57 ± 0.047, $P < 0.0001$, compared to baseline distribution) (Fig. 3E). Consistent with these findings, we also observed a smaller response to direct electrical stimulation in the presence of DHPG in preCGG M neurons compared to Wt (Supplementary Material, Fig. S3).

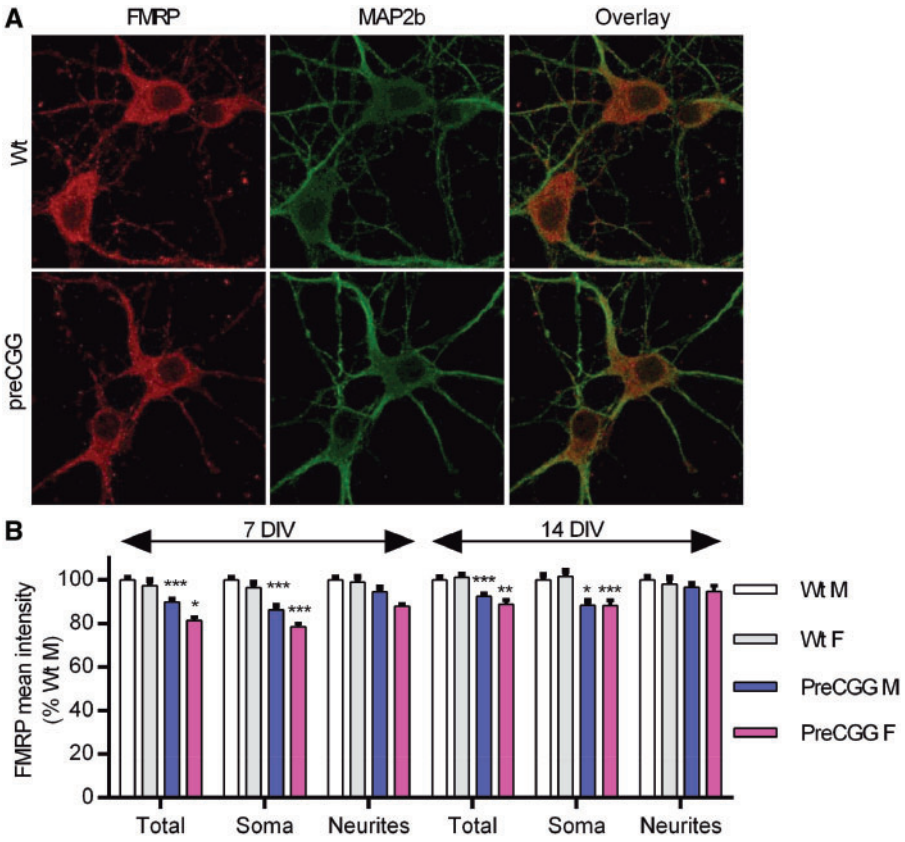

Figure 2. Reduced FMRP is redistributed throughout the neurites in cultured preCGG hippocampal neurons. (**A**) 7 DIV Wt and preCGG cultured hippocampal neurons stained for FMRP (red) and MAP2b (green). (**B**) FMRP fluorescence intensity was quantified in the entire neuron (total), in the soma, and in the neurites of Wt and preCGG male (M) and female (F) hippocampal neurons at 7 DIV and 14 DIV. At 7DIV: 51 Wt M, 11 Wt F, 60 preCGG M and 11 preCGG F hippocampal neurons were measured from 3 differente cultures; For 14DIV: 10 Wt M, 14 Wt F, 8 preCGG M and 15 preCGG F hippocampal neurons were measured from 3 different cultures. Significance was determined using an ANOVA followed by Tukey's multiple comparison test $^{*}P < 0.05$; $^{**}P < 0.01$; $^{***}P < 0.001$. Error bars indicate mean ± SEM.

Elevated resting cytosolic Ca^{2+} in preCGG hippocampal neurons

To examine whether the dysregulated glutamatergic responses observed above could be associated with chronic perturbations in Ca^{2+} homeostasis, we performed simultaneous measurements of the resting cytoplasmic calcium concentration ($[Ca^{2+}]i$) and membrane potential (Vm) with double-barreled microelectrodes. Typical records of Ca^{2+} potential (V_{Ca}) obtained from Wt and preCGG male and females hippocampal neurons, are presented Fig. 4A. As seen from these traces, preCGG neurons exhibited a less negative Ca^{2+} potential than Wt neurons, which corresponds to greater $[Ca^{2+}]_i$ after electrode calibration. Indeed, by culture day 7, preCGG M and F hippocampal neurons already have 2.5- to 3-fold elevation in $[Ca^{2+}]_i$ compared to Wt M and F hippocampal neurons ($[Ca^{2+}]_i$ preCGG M: 317.8 ± 28.7 nM, preCGG F: 272.8 ± 28.1 nM, Wt M: 102.7 ± 3.2 nM, and Wt F: 108.7 ± 4.1 nM, $P < 0.0001$) (Fig. 4B). Elevated $[Ca^{2+}]_i$ in preCGG neurons persists with development. At 14 and 21 DIV, preCGG M and F hippocampal neurons had ~2-fold higher $[Ca^{2+}]_i$ compared to Wt M and F neurons (respectively, 14DIV $[Ca^{2+}]_i$: preCGG M: 259.8 ± 9.6 nM, preCGG F: 238.5 ± 23.0 nM, Wt M: 106.7 ± 1.9 nM, Wt F: 108.4 ± 2.5 nM, $P < 0.0001$; 21 DIV $[Ca^{2+}]_i$: preCGG M: 310.3 ± 21.1 nM, preCGG F: 326.8 ± 30.0 nM, Wt M: 120.1 ± 3.3 nM, and Wt F: 126.5 ± 2.4 nM, $P < 0.0001$) (Fig. 4B).

To verify that basal $[Ca^{2+}]_i$ measurements are not influenced by differences in spontaneous Ca^{2+} oscillations and electrical patterns of activity previously shown to occur in these cultures (14), $[Ca^{2+}]_i$ were repeated in the presence of the Na^{2+} channel blocker tetrodotoxin (TTX, 1 μM) in the recording medium (Fig. 4C). Although the dispersion of the data was reduced, silencing both spontaneous electrical activity and Ca^{2+} oscillations with TTX neither alters the mean of $[Ca^{2+}]_i$ nor the resting membrane potential (Supplementary Material, Fig. S4) in Wt or preCGG hippocampal neurons, as would be predicted from the slow response time of the double-barreled electrodes. Despite chronic elevation of $[Ca^{2+}]_i$ in preCGG neurons, the resting membrane potential (V_m) of premutation neurons was not significantly different from that of Wt neurons for all DIVs measured in control experimental solution (Fig. 4D) or in the solution containing dantrolene (10μM) (Supplementary Material, Fig. S4).

To investigate the possible role of intracellular Ca^{2+} release from ER stores, specifically the leak mediated by ryanodine receptors (RyRs) that could contribute to elevated $[Ca^{2+}]_i$, observed in preCGG, neurons were exposed to dantrolene (10 μM), an inhibitor of RyRs, 10 min prior to recording $[Ca^{2+}]_i$ (Fig. 4B). Cytosolic calcium from Wt M and F neurons showed a modest yet non-significant decrease in presence after 10 min of dantrolene treatment ($[Ca^{2+}]_i$ Wt M + dantrolene: 79.6 ± 2.4 nM, $[Ca^{2+}]_i$ Wt F + dantrolene: 81.0 ± 4.6 nM). However $[Ca^{2+}]_i$ in preCGG M and F neurons at 7 DIV in the presence of dantrolene decreased substantially ($[Ca^{2+}]_i$ preCGG M + dantrolene: 116.9 ± 7.2 nM, $[Ca^{2+}]_i$ preCGG F + dantrolene: 120.2 ± 8.7 nM), achieving basal (without dantrolene) Wt M and F levels at 7 DIV. At 14 DIV,

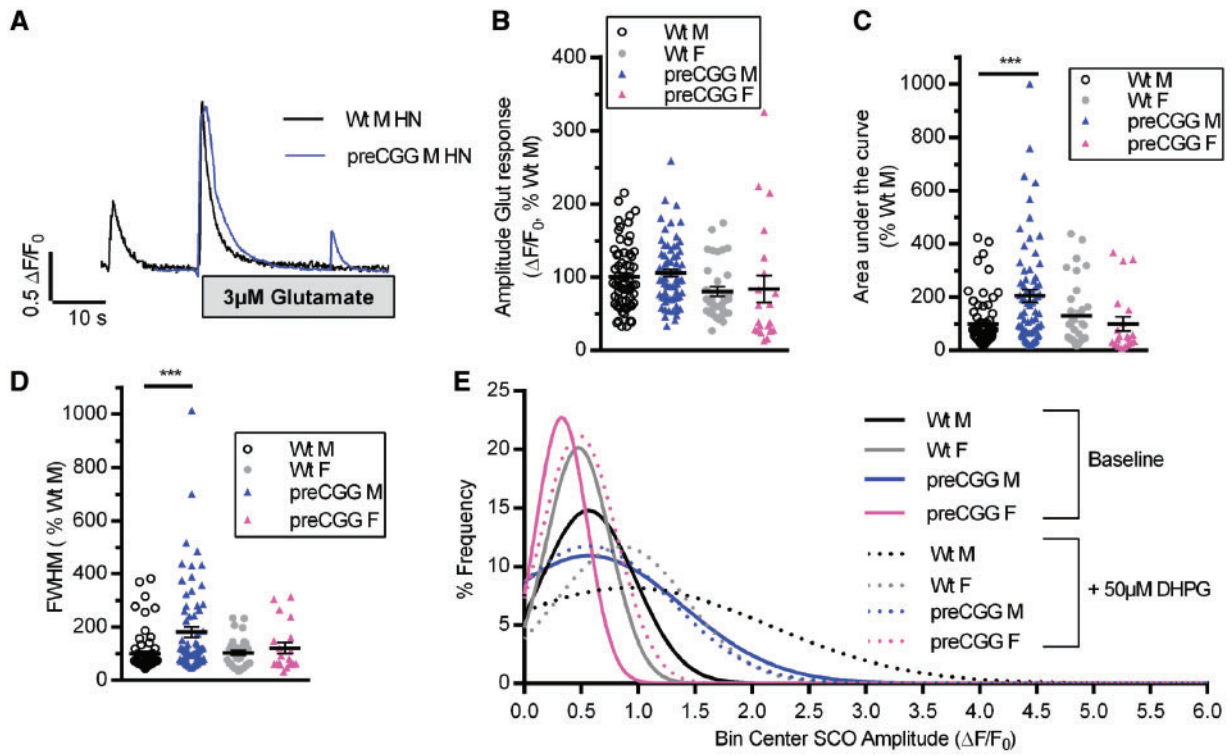

Figure 3. Altered glutamatergic responses in preCGG hippocampal neurons at 14 DIV. (**A**) Representative traces of the Ca^{2+} transient recording in the soma of the neurons in response to the addition of 3 μM glutamate in Wt and preCGG M hippocampal neurons. (**B**) Dot plots with mean and SEM of the maximal amplitude, (**C**) Area under the curve, and (**D**) full width half maximum (FWHM) normalized to Wt M (% of Wt M) measured on the glutamate-induced Ca^{2+} transients of Wt M (black, $n = 65$), Wt F (grey, $n = 34$), preCGG M (blue, $n = 70$), and preCGG F (pink, $n = 20$) hippocampal neurons. (**E**) Non-linear fit of the percentage of frequency distribution of SCO amplitudes during baseline recording (solid line) and after 5 min of incubation with 50 μM DHPG (dotted line) in Wt M ($n = 17$), Wt F ($n = 10$), preCGG M ($n = 17$), and preCGG F ($n = 10$). Significance was determined using an ANOVA followed by Tukey's multiple comparison test for the glutamate-induced Ca^{2+} transient parameters and a Kolmogorov-Smirnov test to compare distribution. ***$P < 0.001$. Error bars indicate mean ± SEM.

dantrolene treatments induced a decrease in $[Ca^{2+}]_i$ of the preCGG M and F neurons without reaching Wt $[Ca^{2+}]_i$ levels. By 21 DIV, preCGG M and F $[Ca^{2+}]_i$ were reduced substantially by dantrolene ($[Ca^{2+}]_i$ preCGG M + dantrolene: 145.4 ± 15.9 nM, $[Ca^{2+}]_i$ preCGG F + dantrolene: 140.2 ± 16.3 nM), approaching basal Wt M and F levels.

Amplified μ-calpain activity in preCGG cortical and hippocampal tissues depresses Cdk5 activation

In order to examine whether the chronic elevated $[Ca^{2+}]_i$ observed in preCGG neurons could influence the μ-calpain signaling pathway, we first measured the expression of this protein in cortical and hippocampal tissues obtained at 3 ages from Wt and preCGG male mice: P_0, 6 weeks old (6 week), and 6 months old (6 months) (Fig. 5A). μ-Calpain expression did not differ among the ages tested nor between genotypes in cortical and hippocampal tissues. μ-Calpain can mediate the degradation of αII-spectrin, a 280 kDa cytoskeletal protein found on the intracellular side of the plasmalemmal membrane, resulting in the formation of two unique and highly stable spectrin breakdown products of 150 and 130 kDa (SBDP150 and 130). Therefore, we used SBDPs as biomarkers for calpain activity and neurodegeneration (44). Although at P_0 preCGG brains show a non-significant trend toward increased SBDP150, by 6 weeks, preCGG cortex and hippocampus, respectively, have 31% and 51% higher SBD150 levels compared to Wt (Fig. 5B). Moreover, elevated SDBP150 further increases by 6 months in preCGG cortical and hippocampal tissues compared to respective Wt (cortex: 206.1 ± 44.5% of Wt control, $P = 0.0377$; hippocampus, preCGG: 209.7 ± 46.7% of Wt control, $P = 0.0379$), implying that preCGG neurons have higher μ-calpain activity.

To verify this conclusion, we performed a direct measurement of μ-calpain activity in cortical and hippocampal lysates from 6 months Wt and preCGG mice (Fig. 5C). Consistent with SDBP150 expression, preCGG cortex and hippocampus had significantly enhanced μ-calpain activity compared to Wt in 6 months M mice (cortex: 151.1 ± 13.7% of Wt control, $P = 0.0032$; hippocampus: 116.8 ± 6.1% of Wt control, $P = 0.0292$). As the over-activation of μ-calpain in preCGG might lead to changes on one of its downstream effector pathways, Cdk5, we measured the conversion of the Cdk5 activator p35 to a pathogenic p25 form, which is dependent on calpain activity *in vivo* (45). Without detectable changes in Cdk5 protein expression (Fig. 6A), 6 week preCGG cortex and hippocampus show an increased p25/p35 ratio compared to Wt, indicating a lower expression of p35 and/or a higher expression of p25 in premutation brains at this age (cortex: 125.4 ± 11.63% of Wt control, $P = 0.0362$; hippocampus: 143.6 ± 14.54% of Wt control, $P = 0.0228$) (Fig. 6B). By 6 months of age, the p25/p35 ratio is 2-fold higher in preCGG cortical and hippocampal tissues than Wt (cortex: 208.3 ± 38.67% of Wt control, $P = 0.0191$; hippocampus: 220.2 ± 64.32% of Wt control, $P = 0.0363$).

A similar trend was observed in 7 DIV cultured hippocampal neurons in which preCGG neurons had increased SDBP150 expression and higher p25/p35 ratio, which could partially be rescued by treatment of the neurons with 10 μM dantrolene

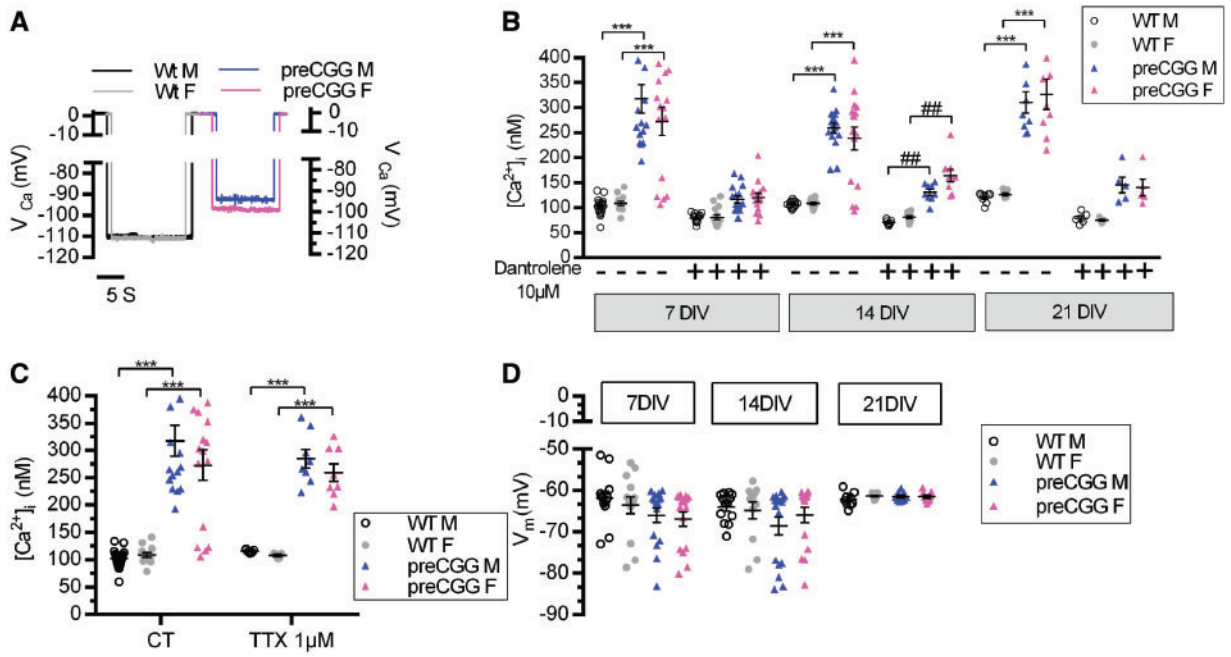

Figure 4. Cytosolic resting calcium concentration ($[Ca^{2+}]_i$) is elevated in preCGG hippocampal neurons. (**A**) Representatives Ca^{2+} potential recording (V_{Ca}) from *Wt* male (*Wt* M), *Wt* female (*Wt* F), preCGG male (preCGG M) and preCGG female (preCGG F) hippocampal neurons. The initial portion of each trace was obtained prior to impalement of the cells. Penetration and removal of microelectrode was accompanied by immediate downward and upward deflection, respectively. (**B**) Dot plot with mean and SEM of $[Ca^{2+}]_i$ values from all *Wt* M and F (respectively for 7, 14 and 21 DIV: $n = 23, 13, 9$ *Wt* M and $n = 14, 12, 9$ *Wt* F) and preCGG M and F (respectively for 7, 14 and 21 DIV $n = 16, 17, 9$ preCGG M and $n = 16, 16, 9$ preCGG F) neurons in Lockes' solution or in presence of dantrolene 10µM (respectively for 7, 14 and 21 DIV: $n = 13, 9, 5$ *Wt* M and $n = 16, 10, 5$ Wt F, $n = 15, 9, 5$ preCGG M and $n = 14, 9, 5$ preCGG F). (**C**) Dot plot with mean and SEM of $[Ca^{2+}]_i$ measurement in paired F and M neuronal cultures from preCGG and *Wt* pups in control (CT) or in the presence of 1 µM TTX at 7 DIV (*Wt* M, $n = 7$, *Wt* F, $n = 8$, preGG M, $n = 10$, preCGG F, $n = 8$). (**D**) Dot plot of membrane potential (V_m) values of paired F and M neuronal cultures from preCGG and *Wt* pups in Lockes' buffer. Significance was determined using an ANOVA followed by Tukey's multiple comparison test. ***$P < 0.001$; ##$P < 0.01$, compared to *Wt* values without dantrolene treatment. Error bars indicate mean ± SEM.

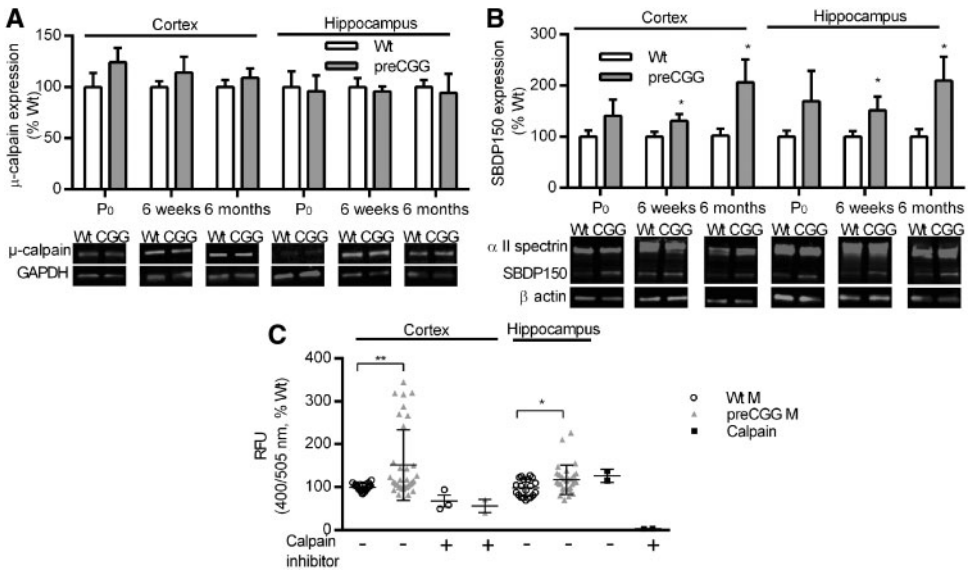

Figure 5. Elevated µ-calpain activity in preCGG cortical and hippocampal tissue lysates. Quantification of (**A**) µ-calpain and (**B**) α II spectrin breakdown products (or SBDP150) expression level relative to GAPDH in cortical and hippocampal tissues of preCGG and age-matched *Wt* mice, normalized to *Wt*. Representative western blots from indicated genotype, brain region, and age are shown below. (**C**) Dot plot of µ-calpain activity using a fluorometric assay in 6-month-old *Wt* ($n = 8$) and preCGG male ($n = 8$) cortical and hippocampal tissue lysates. Cortical lysates incubated with the calpain inhibitor Z-LLY-FMK are showing in the middle. Controls (calpain) with 0.5 µl of calpain are represented at the right of the graphic with or without calpain inhibitor Z-LLY-FMK. The numbers of animals tested is at least, for preCGG cortex: P_0, $n = 7$, 6 weeks, $n = 5$, 6 months, $n = 7$; preCGG hippocampus: P_0, $n = 4$, 6 weeks and 6 months, $n = 5$) and for *Wt* cortex: P_0, 6 weeks and 6 months, $n = 7$; Hippocampus: P_0, $n = 3$, 6 weeks, $n = 7$ and 6 months, $n = 6$). Significance was determined using t-test, *$P < 0.05$; **$P < 0.01$. Error bars indicate mean ± SEM.

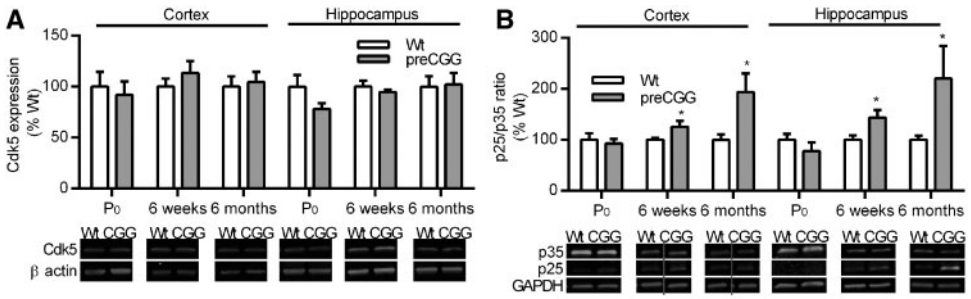

Figure 6. Elevated p25/p35 ratio in preCGG cortical and hippocampal tissue lysates. Quantification of (**A**) Cdk-5 to β-actin and (**B**) the ratio p25/p35 level in cortex and hippocampus of preCGG and age-matched *Wt* mice, normalized to *Wt* expression. Representative western blots from indicated genotype, brain region, and age are shown below. Gels separated by a grey line were run on the same gel but were noncontiguous. The numbers of animals tested is at least, for preCGG cortex: P_0, $n = 7$, 6 weeks, $n = 5$, 6 months, $n = 7$; preCGG Hippocampus: P_0, $n = 4$, 6 weeks and 6 months, $n = 5$) and for *Wt* cortex: P_0, 6 weeks and 6 months $n = 7$; Hippocampus: P_0, $n = 3$, 6 weeks, $n = 7$ and 6 months, $n = 6$). Significance was determined using t-test, $^*P < 0.05$; Error bars indicate mean ± SEM.

(Supplementary Material, Fig. S5A and B). In addition, the ratio p25/p35 is significantly enhanced in human premutation iPSC derived neurons compared to congenic normal iPSC at 7 DIV ($P = 0.0023$) (Supplementary Material, Fig. S6A). Several attempts were made with commercially available antibodies to detect p-Ser^{159}-Cdk5, the activated form of Cdk5, but they failed to show specificity with western blot (data not shown).

ATM and p-Ser^{1981}-ATM upregulation and redistribution in preCGG neurons

Elevated Cdk5/p25 can redistribute to the nucleus, where it phosphorylates several proteins, including the kinase ATM (34–36). We therefore measured the expression level of ATM and its phosphorylated form p-Ser^{1981}-ATM, pointing out ATM activation, in preCGG and *Wt* cortices and hippocampi of male mice (Fig. 7A–D). For all time points, ATM was significantly upregulated, by 1.9-fold and 1.8-fold respectively, in preCGG cortices and hippocampi compared to *Wt* (cortex: 192.9 ± 20.0% of *Wt* control, $P = 0.0040$; hippocampus: 183.1 ± 36.8% of *Wt* control, $P = 0.0372$) (Fig. 7A and D). The same trends were observed for p-Ser^{1981}-ATM at P_0, with a 1.6-fold increase in preCGG cortices compared to *Wt* ($P = 0.0184$); no significant changes were observed, however, in preCGG hippocampi (Fig. 7B and D). At 6 weeks, the upregulation of ATM and its phosphorylated form were attenuated or even absent in the cortex of preCGG mice. However, in the hippocampus of 6-week preCGG animals, the expression of ATM and p-Ser^{1981}-ATM were consistently increased by ∼50% compared to *Wt* (ATM: 150.5 ± 16.9% of *Wt* control, $P = 0.0480$; p-Ser^{1981}-ATM: 145.8 ± 13.1% of *Wt* control, $P = 0.0282$). Finally, the oldest preCGG mice (6 months) exhibited a ∼50% increase in ATM (cortex: 153.6 ± 16% of *Wt* control, $P = 0.0141$; hippocampus: 150.5 ± 16.9% of *Wt* control, $P = 0.0460$) as well as a ∼30–70% increase of p-Ser^{1981}-ATM in both cortical and hippocampal tissue lysates (cortex: 127.2 ± 11% of *Wt* control, $P = 0.0311$; hippocampus: 171.7 ± 23.8% of *Wt* control, $P = 0.0391$) (Fig. 7A–D). In addition, the ratio of p-ATM to total ATM was significantly elevated in preCGG cortical neuronal cultures at P_0 and 6 months (P_0: 140.2 ± 13.1% of Wt, $P = 0.0280$; 6 months: 157.9 ± 19.8% of Wt, $P = 0.0249$) and at all the ages tested in preCGG hippocampal lysates (P_0: 147.2 ± 11.4% of Wt, $P = 0.0099$; 6 week: 150.0 ± 16% of Wt, $P = 0.0235$; 6 months: 143.3 ± 13.8% of Wt, $P = 0.0230$) (Fig. 7C).

A similar trend was observed in 7 DIV cultured hippocampal neurons, with an increase in ATM and p-Ser^{1981}-ATM, which could be partially rescued by treatment of the neurons with 10 μM dantrolene (Supplementary Material, Fig. S5C and D). Furthermore, ATM expression is significantly increased in human premutation iPSC-derived neurons compared to normal iPSC ($P = 0.0423$), and p-Ser^{1981}-ATM expression exhibits a trend to an increase in premutation iPSC-derived neurons compared to normal iPSC (Supplementary Material, Fig. S6B and C).

Phosphorylation of ATM also induces its redistribution from the nucleus to the cytoplasm and, later, to the synaptic terminals (38). Therefore, we studied the localization of p-Ser^{1981}-ATM in 7 DIV preCGG and *Wt* hippocampal neurons using confocal microscopy. p-Ser^{1981}-ATM presents a pattern of intense foci within nuclear vesicles (Fig. 7E, white arrows), with a higher number of foci per cell in cultured preCGG neurons compared to *Wt* (Fig. 7E and F, $P = 0.0362$); p-Ser^{1981}-ATM staining was also found spread along the soma and the neuronal arborization in preCGG neurons. The ratio between the mean intensity of p-Ser^{1981}-ATM measured in the cytoplasm of the neurons (soma + neurites) versus that measured in the nucleus was higher in preCGG hippocampal neurons (Fig. 7E and F, $P = 0.0224$), indicating a clear distribution in favor of the cytoplasm in premutation neurons.

Imbalance of pro-apoptotic/pro-survival markers in preCGG neurons

The Cdk5-ATM signaling pathway involves the regulation of p53 (34), known to activate the expression of many essential downstream target genes related to cell death, including the pro-apoptotic protein Bax (46). We measured the expression of Bax and compared it to the expression of the pro-survival protein, Bcl-2, in *Wt* and preCGG cortical and hippocampal tissues (Fig. 8A and B). At the early developmental stages (P_0 and 6 week), preCGG and *Wt* cortices and hippocampi showed no significant differences in the pro-apoptotic/pro-survival balance. Interestingly, at 6 months old, preCGG animals had a higher Bax/Bcl-2 ratio in the cortex (∼25% increase; $P = 0.0305$) and hippocampus (∼30% increase; $P = 0.0298$) compared to *Wt* animals. This suggests that preCGG brains have an upregulation of Bax and/or a downregulation of Bcl-2 proteins, indicating a greater vulnerability to apoptosis, as a late-onset component of the CGG-repeat-mediated disorder. A similar trend was observed in 7 DIV cultured hippocampal neurons with an increase in the Bax/Bcl-2 ratio, which could be partially rescued by treatment of the neurons with 10 μM dantrolene (Supplementary Material, Fig. S5E).

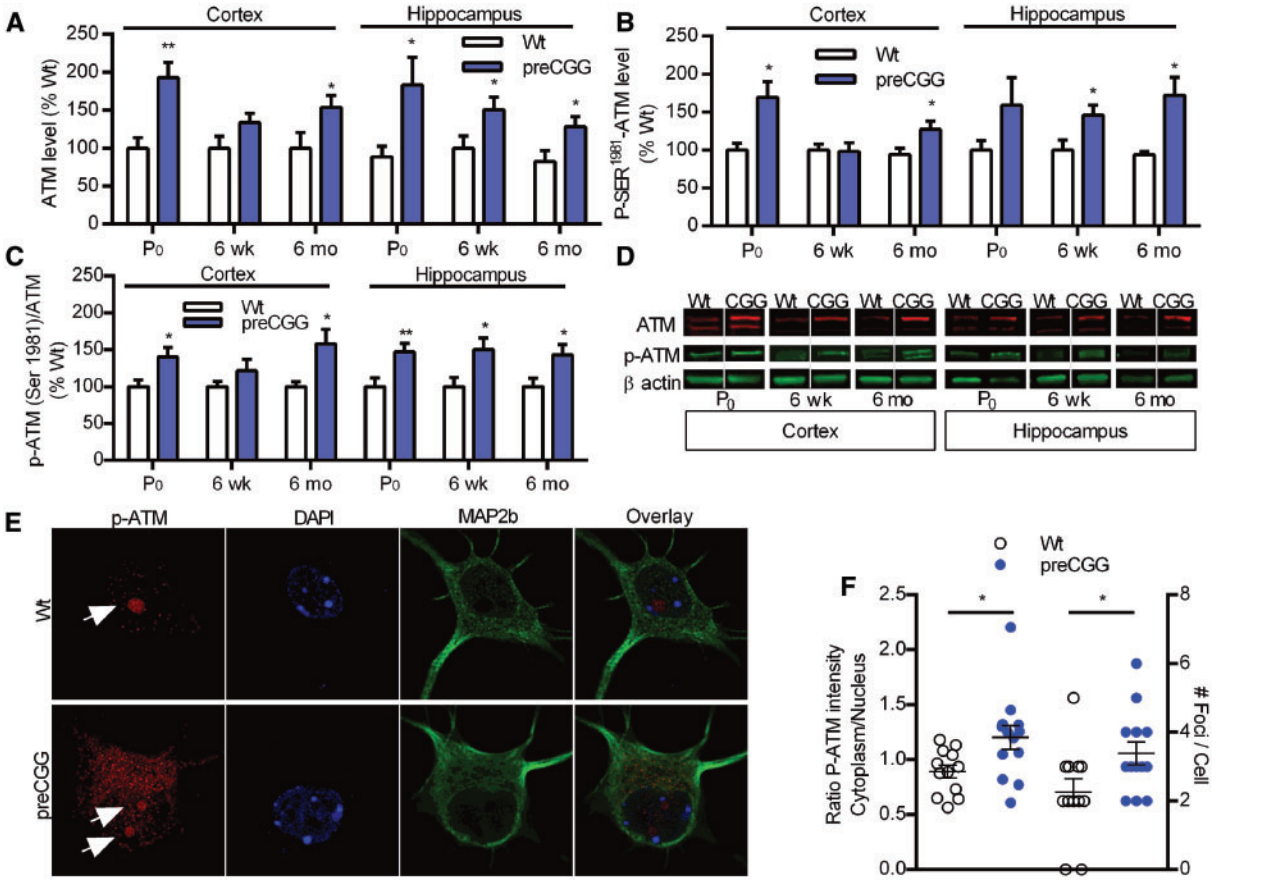

Figure 7. ATM and p-Ser1981-ATM upregulation and redistribution in preCGG neurons. Quantification of ATM (**A**) and p-Ser1981-ATM (**B**) expression level relative to β-actin in cortical and hippocampal lysates of preCGG (Cortex: P_0, $n = 8$, 6 weeks and 6 months, $n = 7$; Hippocampus: P_0, $n = 6$, 6 weeks, $n = 7$ and 6 months, $n = 5$) and age-matched Wt mice (Cortex: P_0, $n = 6$, 6 weeks and 6 months, $n = 5$; Hippocampus: P_0, $n = 6$, 6 weeks, $n = 8$ and 6 months, $n = 5$), normalized to Wt. (**C**) Quantification of the ratio of p-Ser1981-ATM to ATM in cortical and hippocampal lysates of preCGG (Cortex: P_0, $n = 8$, 6 weeks and 6 months, $n = 7$; Hippocampus: P_0, $n = 6$, 6 weeks, $n = 7$ and 6 months, $n = 5$) and age-matched Wt mice (Cortex: P_0, $n = 6$, 6 weeks and 6 months, $n = 5$; Hippocampus: P_0, $n = 6$, 6 weeks, $n = 8$ and 6 months, $n = 5$) normalized to Wt. (**D**) Representative ATM (upper row), p-Ser1981-ATM (middle row), and β-actin (lower row) western blots from indicated genotype, brain region, and age. Gels separated by a grey line were run on the same gel but were noncontiguous. (**E**) Immunolocalization of p-Ser1981-ATM (red) forming foci (indicated by white arrows) in the nucleus (DAPI, blue) in hippocampal neurons labeled with MAP2b (green) in Wt (upper panel) and preCGG (lower panel) hippocampal neurons at 7 DIV. Bar = 6 μm. (**F**) Dot plot with mean and SEM of the average intensity of p-Ser1981-ATM in the cytoplasm relative to the intensity in the nucleus (left side of the figure) in Wt ($n = 12$) and preCGG ($n = 13$) hippocampal neurons; number of p-Ser1981-ATM foci per nucleus in each cell (right side of the figure) in Wt ($n = 12$) and preCGG ($n = 13$) hippocampal neurons. Significance was determined using t-test $^*P < 0.05$; $^{**}P < 0.01$. Error bars indicate mean ± SEM.

Elevated reactive oxygen species (ROS) in preCGG neurons

Reactive oxygen species (ROS), such as superoxide anion (O_2^-), hydrogen peroxide (H_2O_2), and hydroxyl radical (HO•), consist of radical and non-radical oxygen species formed by the partial reduction of oxygen. Additional cellular ROS can be generated endogenously when the Bax/Bcl-2 balance is dysregulated or when there is a chronic cytosolic Ca^{2+} overload observed in many neurodegenerative disorders (43,47,48). Therefore, we investigated whether preCGG neurons exhibit alterations in ROS levels. Using the ROS dye CellROX® Green, we assessed the ROS levels in Wt and preCGG M and F hippocampal neurons at rest without any external stress (Fig. 9A and B). As shown in Fig. 9A, CellROX® Green primarily labels the nucleus and the soma of the cells when it reacts with ROS; this can be quantified using automated high-throughput imager software (ImagXpress) by measuring the average fluorescence intensity per image, normalized by the number of cells using nuclear DAPI staining. We observed that even though resting Ca^{2+} overload was already present at 7 DIV, there was no significant increase in basal ROS in preCGG hippocampal neurons (Fig. 9A and B). However, at 14 DIV, basal ROS was ~30% higher in preCGG M neurons compared to Wt M, while preCGG F basal ROS stress remained similar to Wt F. By culture day 21, basal ROS remained enhanced in preCGG M by ~20% compared to Wt, and preCGG F showed a trend toward higher ROS as well (Wt M: 100 ± 6.8%, Wt F: 95 ± 2.9%, preCGG M: 116.9 ± 8.5%, preCGG F: 112.6 ± 4.8%). Similar to the $[Ca^{2+}]_i$ recording experiments, we exposed the neurons to dantrolene (10 μM) during 10 min in the culture media. The presence of dantrolene for all DIV time points induced a general decrease in the level of ROS for all genotypes and was sufficient to rescue basal ROS to Wt levels in preCGG M neurons at 14 and 21 DIV.

We examined cells when challenged by 1,4-naphtoquinone to generate ROS through redox cycling and depleting glutathione in exposed cells and tissues (49). As shown in Fig. 9C, we were able to follow in real time the level of CellROX® Green fluorescence and its time-course in response to 1,4-naphthoquinone (1–100 μM) in

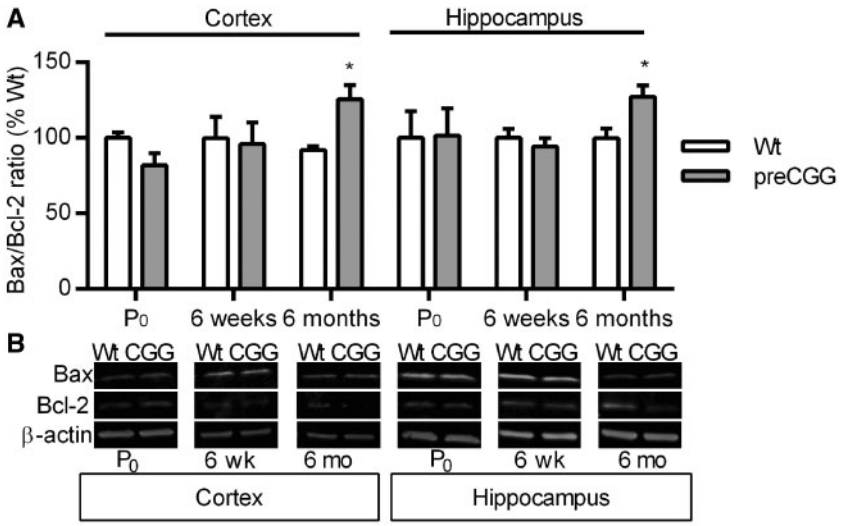

Figure 8. Ratio of Bax to Bcl-2 is elevated at 6 months in preCGG cortices and hippocampi. (**A**) Quantification of the ratio Bax/Bcl-2 in cortical and hippocampal lysates of preCGG (Cortex: P_0, $n=4$, 6 weeks, $n=3$, 6 months, $n=4$; Hippocampus: P_0, 6 weeks and 6 months, $n=4$) and age-matched Wt mice (Cortex: P_0, $n=4$, 6 weeks and 6 months, $n=3$; Hippocampus: P_0, 6 weeks and 6 months, $n=4$), normalized to Wt. (**B**) Representative Bax (upper row), Bcl-2 (middle row), and β-actin (lower row) western blots from indicated genotype, brain region, and age. Significance was determined using t-test $^*P<0.05$. Error bars indicate mean ± SEM.

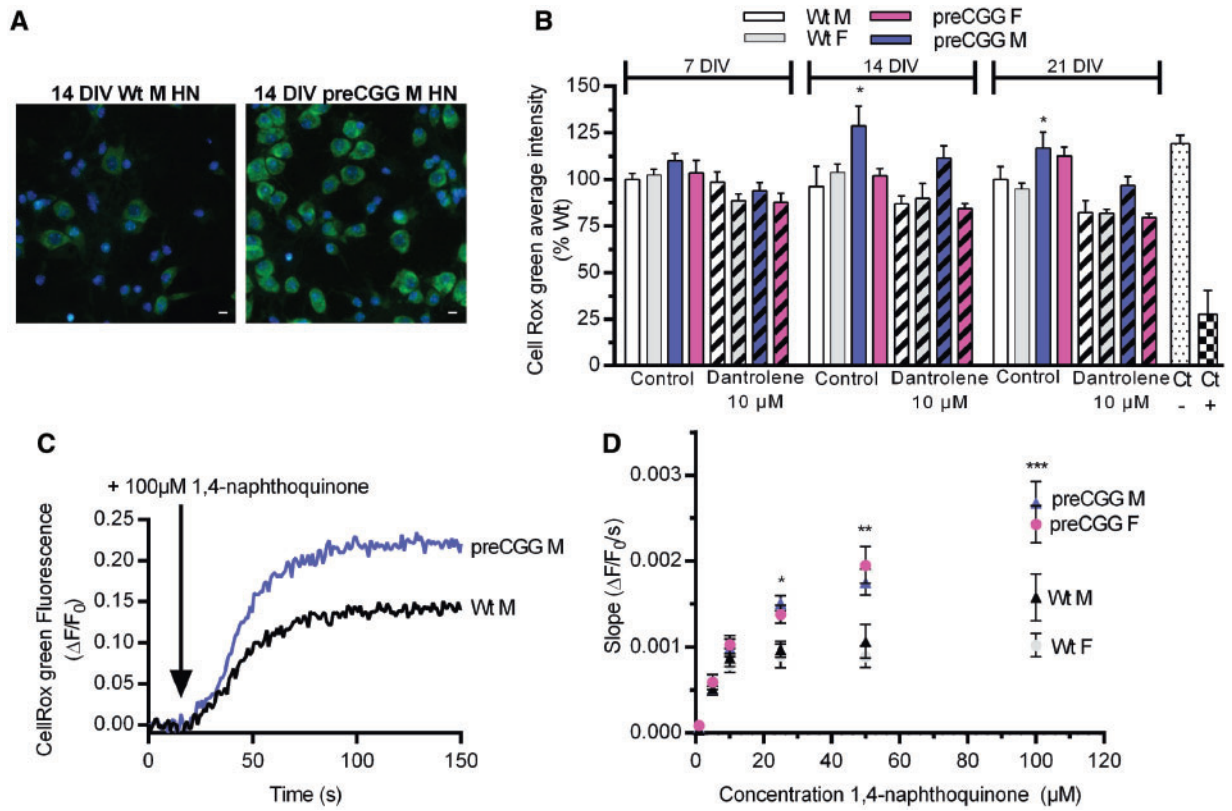

Figure 9. Elevated ROS level in preCGG hippocampal neurons. (**A**) Representative pictures of Wt and preCGG hippocampal neurons (HN) after 30 min CellROX® Green (green staining) incubation under control conditions. Nuclei are labeled in blue. Bar = 3μM. (**B**) Dot plot of the basal ROS level using CellROX® Green fluorescence measurement in paired cultures of M and F Wt and preCGG HN under control conditions (plain bar) and in the presence of 10 μM dantrolene in the media (striped bar). 50 μM 1,4-naphthoquinone was used as a positive control (CT +) and 100 μM N-acetylcysteine as a negative control (CT -). $N=3$ separated cultures with 3 or 4 wells for each experimental group. (**C**) Representative traces of the live measurement of CellROX® green fluorescence in Wt and preCGG HN at 7 DIV. Addition of 100 μM 1,4-naphthoquinone induced a faster increase in fluorescence in preCGG HN compared to Wt. (**D**) Quantification of the rate of increase (slope) in the first 60 s following the addition of several 1,4-naphthoquinone concentrations to Wt and preCGG male and female HN. Vehicle was also added as a control (2% DMSO) without any changes in fluorescence level (data not shown). $N=3$ separated cultures with 3 wells for each experimental group. Significance was determined using an ANOVA followed by Tukey's multiple comparison test $^*P<0.05$; $^{**}P<0.01$; $^{***}P<0.001$. Error bars indicate mean ± SEM.

7 DIV Wt and preCGG hippocampal neurons. 1,4-Naphthoquinone less than 25 μM induced a similar initial rate of rise in fluorescence signal with Wt and preCGG hippocampal neurons. However, >25 μM 1,4-naphthoquinone produced a nearly 2-fold higher initial slope of fluorescence rise in preCGG M neurons compared to Wt M. Similarly, the slope of fluorescence increase in preCGG F neurons did not differ from Wt F at <25 μM 1,4-naphthoquinone but was ∼2-fold greater than Wt at the higher concentrations tested (Fig. 9D).

Discussion

Results from the present study provide several mechanistic chronological clues linking early abnormalities in Ca^{2+} dynamics with critical elements of the neuronal DDR in the Rotterdam *FMR1* preCGG mouse model (11) (Fig. 11). The earliest manifestation is aberrant neocortical neuronal migration detected as early as embryonic day 16 (9), a Ca^{2+}-regulated process (50). Here we show that chronically elevated neuronal $[Ca^{2+}]_i$ is a hallmark of preCGG neurons isolated from neonate mice as early as 7 DIV in cells that are forming networks, an early window into their *in vitro* developmental trajectory before neuronal connectivity has been fully established. In fact, preCGG cultured neurons have been documented to exhibit reduced dendritic complexity and abnormal synaptic architecture beginning in early development at 7 DIV (10,12). As expected, abnormal neuronal $[Ca^{2+}]_i$ dynamics have been associated with neuronal mitochondrial dysfunction as early as 4 DIV, with significantly reduced numbers and showing a greatly reduced mobility in preCGG compared to Wt (51). Interestingly, this takes place before measurable evidence of increased ROS production, loss of cell viability, or biomarkers of neurodegeneration. These early abnormal indicators, consistent with neuronal $[Ca^{2+}]_i$ dysregulation, are temporally coincident with sustained overexpression of *FMR1* mRNA and reduction in FMRP, two defining hallmarks of human premutation (10,15,16, 20,52–55).

It is reasonable to hypothesize that chronically elevated $[Ca^{2+}]_i$ commencing early in brain development would promote adaptive and potentially injurious sequelae that would have impacts on synaptic signaling once networks are consolidated and mature, evidenced by abnormal mGluR1/5 responses, as well as influences on regulation of the DDR. The possible link between abnormal mGluR signaling and chronically elevated cytoplasmic $[Ca^{2+}]_i$ observed in preCGG neurons is likely to involve both transcriptional and post-transcriptional mechanisms. Steady-state intracellular Ca^{2+} levels, synchronous Ca^{2+} oscillations, and Ca^{2+} signals elicited by excitatory neurotransmission all play significant roles in transcriptional regulation of synaptic proteins, metabolism, neuronal plasticity, and neuronal survival (56).

An interesting observation is the sex differences in SCO patterns observed within the same genotype. Such differences could be explained by endocrine influences already manifest on P_0 when cultures are established. For example, estrogen is known to influence hippocampal function through multiple mechanisms, with time courses ranging from minutes to days. Hippocampal neurons express the E2-synthesizing enzyme P450 aromatase, which could provide a source of locally generated E2 to modulate synaptic function during *in vitro* development (57,58).

Dantrolene is an antagonist of the RyR-mediated Ca^{2+} signaling (59), which has been used to protect against neuronal damage in spinocerebellar ataxia (60) and Huntington's disease (61). Considering its noted inhibitory effects on RyRs, glutamate excitotoxicity (62), and ROS (63), it is not surprising to see that incubation of preCGG neurons with 10μM dantrolene for 10 min was sufficient to recover resting $[Ca^{2+}]_i$ to levels comparable to Wt, suggesting a dysfunction of the intracellular Ca^{2+} homeostasis, particularly at the level of RyRs channels. Although dantrolene caused a trend towards normalization of key proteins regulating the Cdk5-ATM pathway in cultured hippocampal neurons, the difference was not statistically significant, which may be explained, at least in part, by the short exposure time to the drug, or the irreversible nature of Cdk5-ATM dysregulation, once changes in the pathway have already manifested. It is also reasonable to speculate that a more prolonged exposure to dantrolene before the initiation of pathological features in preCGG neurons could more significantly normalize the Cdk5-ATM pathway.

A complete loss of FMRP in fragile X syndrome clearly indicates this protein is an essential regulator of both local synaptic protein synthesis within dendrites and activity-dependent changes in synaptic plasticity mediated by Group 1 mGluR (15,64–66). However, partial downregulation of FMRP in specific regions of the developing brain cannot fully explain the early onset of biomarkers of neuronal dysfunction and cognitive impairments (7) and their slow progression to the neurodegenerative features of FXTAS. Importantly, the absence of the neurodegenerative phenotype in adults with fragile X syndrome (and absence of FMRP and its mRNA) indicates that partial loss of FMRP cannot be a primary effector of FXTAS. In support of this, our *in vitro* results with iPSC-derived neuronal lines, derived from a chimeric premutation female having expanded (premutation) or normal CGG repeats, show indistinguishable levels of FMRP (Supplementary Material, Fig. S2), but the human premutation neurons exhibit several abnormal growth (e.g., reduced neurite growth) and signaling deficits (e.g., abnormal glutamatergic responses), consistent with the mouse preCGG model (16,17). Moreover, our sub-cellular localization data show that FMRP in cultured preCGG neurons is downregulated in the soma but not significantly different in the neurites (axon, proximal and distal dendrites). The fact that FMRP is measurably lower in soma but not dendrites of preCGG neurons could reflect a compensatory mechanism by which preCGG neurons rebalance the mild downregulation of FMRP by redistributing it from soma to dendritic regions where it plays a crucial role for neuronal plasticity and activity. Indeed, FMRP is an RNA-binding protein and a repressor of translation, regulating dendritic mRNA translation, required for multiple forms of plasticity (64,66,67). FMRP itself is dynamically regulated by activity: experience and synaptic activation can trigger its local translation and rapid degradation, in addition to the posttranslational regulation mentioned above. Also, in hippocampal cultures, activity- and mGluR-dependent increases in dendritic FMRP may result from increased trafficking of existing FMRP, rather than *de novo* FMRP synthesis (67). FMRP participates in receptor localization/internalization by regulating the translation of receptor-binding proteins, such as PSD-95 (68), and Homer scaffolds within the postsynaptic density (65). Therefore, relocalization of FMRP is an essential homeostatic control point for maintaining appropriate synaptic activity. Finally, as GGGGCC repeat RNA has been suggested to disrupt FMRP-mediated translational repression or increase FMRP-mRNA target stability (69), we can also hypothesize that CGG repeat overexpression could influence FMRP localization to neurites within preCGG neurons.

Collectively, these data suggest that elevated *Fmr1* mRNA and/or co-transcriptional events such as R-loop formation (70), rather than reductions in FMRP, may be etiologically more important in promoting early signaling and morphometric defects

observed with *FMR1* premutations. The elevated *Fmr1* mRNA measured could lead to an increase in R-loop formation and RNA-binding proteins, resulting in activation of DDR as early as P_0, consistent with the upregulation of ATM and it is phosphorylated form at this time point, despite the lack of intranuclear inclusions formation in cultured hippocampal neurons at this stage of development (21,27,70,71).

In addition to the evidence for a role of *Fmr1* mRNA gain of function toxicity (19–21), recently, a repeat associated non-ATG (RAN) translation sequence has been implicated in preCGG neuropathology. In this model, a CGG repeat expansion triggers the RAN translation of a cryptic polyglycine-containing protein, FMRpolyG; the RAN product is reported to be present in ubiquitinated neuronal intranuclear inclusions in FXTAS patient brains (28,31). Whether one or both of the above mechanisms are necessary and sufficient for promoting chronically elevated neuronal $[Ca^{2+}]_i$ remains to be determined. However, it should be noted that low but detectable levels of FMRpolyG can be detected in brain regions of *Wt* mice, and levels are only elevated in aged (18 mo) preCGG mice (28).

Here we provide the first evidence, from primary neuronal cultures in *in vitro* and *in vivo* cortical and hippocampal tissues from preCGG mice, of chronically elevated μ-calpain activity and a downstream consequence of enhanced Cdk5-ATM signaling factors that are critical for regulating both neuronal DDR and synaptic plasticity. Indeed, our data points to the conclusion that the Ca^{2+} overload in preCGG neurons significantly contributes to neuronal dysfunction through activation of μ-calpains, localized in the cytoplasm as an inactive proenzyme. μ-calpain is activated in the presence of high levels of Ca^{2+} (0.2–80 μM), which is in the range of the resting $[Ca^{2+}]_i$ measured in preCGG hippocampal neurons. Indeed, preCGG cortices and hippocampi display at 6 weeks of age an over-activity of μ-calpain without any changes in the expression of the enzyme. The activity of calpain is widely implicated in a broad range of pathologies such as Alzheimer's (72), Parkinson's (73), and Huntington's diseases (74). Reinforcing this idea, we also found an increase of the conversion of p35 to p25 in 6-week-old preCGG mice, a process controlled by μ-calpain. This cleavage of p35 to p25 increases the kinase activity of Cdk5 while relocating the complex to the nucleus, common to other neurodegenerative processes (33). The Cdk5/p25 complex has numerous functions, among them the phosphorylation of lamin A/C, which has been found in the intranuclear inclusions of FXTAS cases (55–26). Neural cells transfected with expanded CGG-repeat plasmids have shown a disruption of the nuclear lamin ring architecture and the formation of inclusions containing lamin A/C (31–55).

More recently, a new target emerged whereby Cdk5/p25 directly phosphorylates ATM at Ser^{794}, a process required for auto-phosphorylation at Ser^{1981} and subsequent activation of ATM kinase activity (34–36). In the current context, the upregulation of ATM, and particularly of its phosphorylated form at Ser^{1981} at 6 weeks and 6 months of age, matches with the elevated p25/p35 ratio observed in preCGG brain at the same development period. However, at P_0, p-Ser^{1981}-ATM is upregulated while the p25/p35 ratio in preCGG mice is unchanged. Those observations suggest that, at this point of development, DNA damage, a possible consequence of the greater propensity of R-loop formation on premutation alleles (26,27,70,75), may be a major activator of the ATM signaling pathway. In addition, there are several non-DDR functions of ATM that converge to regulate the cellular response to ROS, suggesting that elevated $[Ca^{2+}]_i$ and increased production of ROS observed in preCGG neurons as early as 7DIV also directly influence ATM activity (39,76) at this early period of the brain development.

Although ATM is a predominantly nuclear protein, it plays an important role as a cytoplasmic protein in neurons and specifically in synaptic function (38). Interestingly, p-Ser^{1981}-ATM has a higher density in the cytoplasm of the preCGG neurons compared to *Wt* as early as 7DIV. Bicuculline-induced synaptic activation can produce a similar increase of p-Ser^{1981}-ATM in the cytoplasm in neurons, suggesting that ATM redistribution could be linked to the abnormal synaptic activity observed in preCGG neurons (77). Moreover, activity-dependent redistribution of p-Ser^{1981}-ATM to the cytoplasm has been recently shown to phosphorylate a subset of serine/threonine-glutamine (SQ) neuronal proteins that include receptors and channels (77). Thus, in the current context, ATM kinase might SQ-phosphorylate several channels and/or receptors reinforcing the Ca^{2+} dysregulation observed in our study. Therefore, early upregulation of p-Ser^{1981}-ATM associated with a more cytoplasmic distribution in premutation KI neurons could be involved in the glutamatergic dysregulation observed. Moreover, the contribution of the Cdk5-ATM pathway in early neuronal dysfunction in premutation carriers is strengthened by the elevated p25/p35 ratio and ATM level found at 7DIV in iPSC-derived from a mosaic human premutation carrier, previously reported to exhibit aberrant Ca^{2+} activity (17). The key proteins of the Cdk5/ATM pathway observed in our preCGG KI mouse model can be translated to human cells.

The later alteration of the pro-apoptotic/pro-survival balance toward apoptosis, measured by the ratio of Bax to Bcl-2 in preCGG brain, reveals a higher vulnerability to apoptosis of those cells. In agreement with our findings, glutamate-mediated cell death leads to a significant decrease in Bcl-2 levels alongside an upregulation of Bax in a neuronal cell line (78). In addition, p53, well known to be activated by ATM, can influence the expression and/or the activity of Bax (46). Ca^{2+} overload in neuronal cells that exceeds the buffering capacity of the mitochondria can interfere with electron transport yielding ROS, and thus impair the activities of transcription factors and, ultimately, induce the downregulation of Bcl-2 combined with an increase in Bax and apoptosis via mitochondrial-mediated mechanisms (48). The late changes in Bax/Bcl2 ratio suggest that elevated ROS production observed from 7 DIV in preCGG neurons followed by an elevated basal ROS level can be explained by mitochondrial dysregulation caused by the early chronic cytosolic Ca^{2+} overload observed in preCGG neurons. In addition, our observations are consistent with several studies from cultured dermal fibroblasts and brain samples from premutation carriers, showing a lower expression of mitochondrial proteins, a lower oxidative phosphorylation capacity, and a higher production of ROS (79–81).

Although the Ca^{2+} overload associated with the activation of Cdk5-ATM pathway is clearly involved in early abnormal neuronal growth and synaptic function in *FMR1* premutation, we cannot exclude the possible involvement of FMRpolyG at CGG repeats later in life. FMRpolyG can be subsequently accumulated in *FMR1* premutation cells and alter neuronal proteostasis that contributes to pathogenesis in FXTAS (28–30). For instance, accumulation of RAN translation products has been linked to dysfunction in Ca^{2+} homeostasis and reduced levels of the anti-apoptotic protein Bcl-2 in iPSCs derived from fibroblasts of patients carrying Amyotrophic Lateral Sclerosis mutation (82,83).

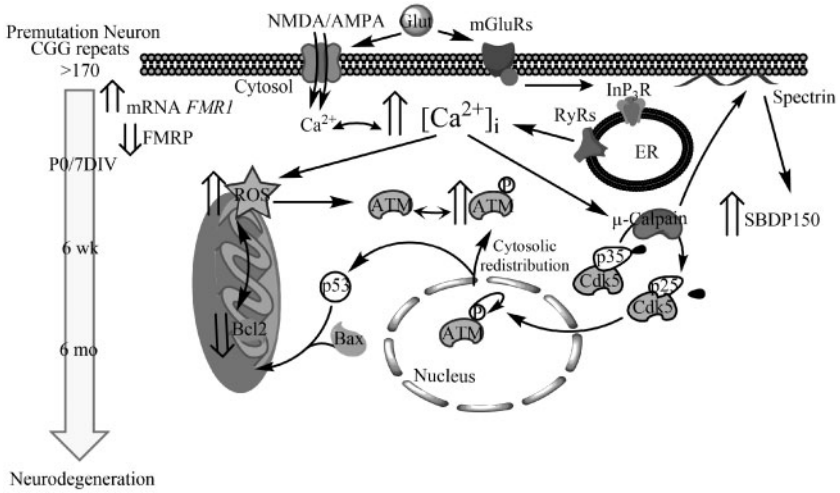

Figure 10. Working model for early events occurring in premutation neurons. Premutation neurons exhibit an early chronic elevated $[Ca^{2+}]_i$ associated with Ca^{2+} signaling dysregulation. This early Ca^{2+} overload leads to mitochondrial dysfunction yielding to an excessive ROS production that can activate ATM. Around 6 weeks of age, elevated $[Ca^{2+}]_i$ increases the activity of the μ-calpain, inducing a degradation of spectrins at the inner membrane and a activation of Cdk5 through the cleavage of p35 in p25. Cdk5 migrates then in the nucleus to phosphorylate substrates and among them, ATM. P-ATM redistributes in the cytosol where it can act on channels amplifying the Ca^{2+}. Later on, P-ATM activates p53 which induces the recruitment and increase in Bax and ultimately induces the downregulation of Bcl-2, causing apoptosis via mitochondrial-mediated mechanisms. Not shown in this figure are late stages of the neurodegenerative process that include the formation of intranuclear inclusions, and the possible participation of RAN-mediated events.

Finally, the novelty of the study is a direct measurement of a $[Ca^{2+}]_i$ overload in preCGG neurons, which occurs early, well before any evidence of neuropathology, unlike other degenerative disorders as in Alzheimer's disease (84), Huntington's disease (85), or in neurons from Duchenne muscular dystrophy mouse models (86), where the Ca^{2+} overload is concomitant with the neuropathology.

In conclusion, our findings show that early chronic Ca^{2+} dysregulation amplifies Cdk5-ATM signaling pathway activity, possibly linking abnormal synaptogenesis with impaired DDR associated with mitochondrial dysfunction in premutation carriers (Fig. 10). We propose that chronic Ca^{2+} dysregulation amplifies the Cdk5-ATM signaling pathway, possibly linking early abnormal $[Ca^{2+}]_i$ with abnormal mGluR1/5 synaptic signaling and DDR that could drive neurodegenerative sequelae that promote clinical FXTAS. This pathway is involved in early neuronal network abnormalities and could serve as new targets for the prevention or retardation of neurodegenerative sequelae of *FMR1*-expansion disorders. A direct causality link between the mechanisms identified here and the pathogenesis of FXTAS deserves further investigation.

Materials and Methods

PreCGG mouse model

All preCGG KI and wild type (Wt) mice in the C57BL/6 background were housed under standard vivarium conditions. PreCGG hemizygous male and homozygous female pups (115–205 CGG repeats, average 172) were obtained by breeding homozygous preCGG females with preCGG hemizygous males. Unlike humans, mice with more than 200 CGG repeats do not have hypermethylated FMR1 alleles and continue to produce FMRP. Male and female Wt pups delivered on the same day as preCGG pups were used separately for paired control cultures, pooling pups of the same sex and genotype, to investigate possible differences. All animal use protocols were approved by the IACUC at the University of California, Davis.

Genotyping

DNA was extracted from the ear punch or tail of individual mice and genotyping of *Fmr1* expansion size was performed by GenoTyping Center of America (GTCA, Ellsworth, ME). The *Fmr1* locus was detected utilizing PCR (Forward: GCTCAGCTCCG TTTCGGTTTCACTTCCGGT, Reverse: CAGGCGCTTGAGGCCCA) followed by gel electrophoresis. The reaction was run on a Roche LightCycler 480 with conditions suggested for Accustart II taq (QuantaBio, Beverly, MA). Analysis was performed after running the amplicons on a 2% agarose gel. Band sizes were estimated based upon the migration of a known DNA Ladder.

Primary cultures of mouse hippocampal neurons

Hippocampal neuron cultures were obtained from postnatal day 0–1 (P_0–P_1) Wt or preCGG KI male and female pups. Dissected hippocampi were incubated for 30 min at 37 °C in a solution of 0.25% Trypsin-EDTA (Gibco™, Thermo Fisher, Waltham, MA) and then washed in a Krebs solution containing 0.6 mg/ml of trypsin inhibitor and 80 μg/ml DNAse (Sigma, St. Louis, MO) before dissociating the cells with a fire-polished Pasteur pipette. Cells in the supernatant were spun down (7 min, 1400 rpm) and resuspended in growth medium (Neurobasal Medium (Gibco™, Thermo Fisher) containing GS21™ neural supplement (MTI-GlobalStem, Gaithersburg, MD), and 0.5 mM Glutamax (Gibco™, Thermo Fisher) with 5% fetal bovine serum (Gibco™, Thermo Fisher), counted and plated onto a 1% (w/v) poly-L-lysine-coated 6- or 24-well plates (TPP Techno Plastic Products®, Trasadingen, Switzerland) or clear-bottom, black well, 96-well imaging plates (Falcon, Corning incorporated, Tewksbury, MA) with 1 x 10^6 cells/well, 2 x 10^5 cells/well or 5 x 10^4 cells/well, respectively. For immunofluorescence

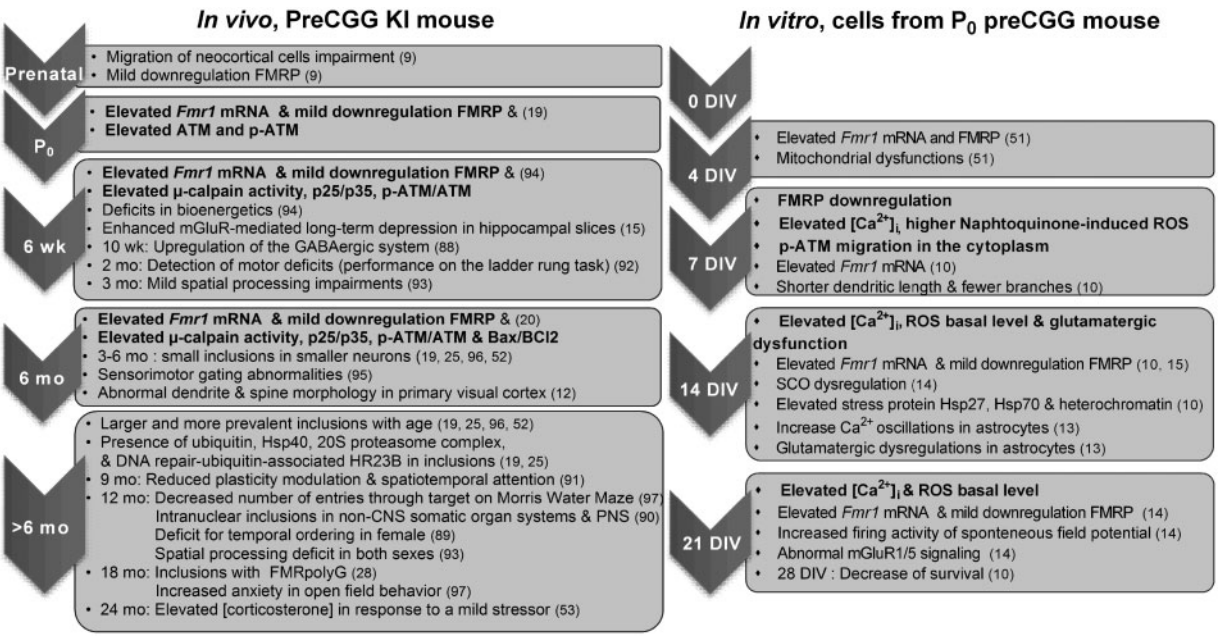

Figure 11. Chronology of *Fmr1* premutation neuropathology *in vivo* and *in vitro* using the Dutch preCGG KI mouse, including the literature and our findings (bold). The left panel summarizes the chronological events occurring *in vivo* in preCGG KI mouse model reported in the literature and in our study (bold). The right panel summarizes the chronological events occurring *in vitro* in cultured neurons from preCGG KI mouse reported in the literature and in our study (bold). Additional citations, not mentioned in the text have been added: (88–97).

experiments, cells were seeded on a sterile glass coverslip pretreated with nitric acid before coating with PLL. Two hours after seeding, the serum level was diluted by half with the addition of serum-free growth medium. 5 µM of cytosine β-D-arabinofuranoside (Ara-C, Sigma) was added at DIV 2 to stop the proliferation of astrocytes. The cells were maintained in an incubator at 37 °C with 5% CO_2.

Western blot

Flash-frozen cortex and hippocampus tissues from P_0, 6-week-, and 6-month-old male preCGG and age matched *Wt* mice were homogenized with an electric homogenizer in modified RIPA buffer (150 mM NaCl, 50 mM Tris pH: 7.4, 1% Triton X-100, 0.5% Na deoxycholate, 0.1% SDS, 5 mM EDTA, 2 mM EGTA, 1X Roche Complete Protease and 1X Roche phosphatase inhibitors). Hippocampal neurons in culture were collected in modified RIPA. Lysates were incubated for 30 min on ice and then spun down by centrifugation at 20,000 rpm for 20 min at 4 °C. Protein concentrations were determined by BCA method (Thermo Scientific, Waltham, MA). Proteins (50 µg per lane for brain and 15 µg for cell culture) were separated using SDS-PAGE 4-15% gradient gels (Bio-Rad, Hercules, CA) and transferred to PVDF or nitrocellulose membranes. Membranes were then blocked with Odyssey blocking buffer (Li-Cor Biosciences, Lincoln, NE) with 0.2% Tween-20 and incubated overnight at 4 °C with primary antibodies: monoclonal FMRP 1/500 (clone 1C3) (Millipore, Billerica, MA), polyclonal µ-calpain large subunit 1/1000 (#2556, Cell Signaling, Danvers, MA), monoclonal α fodrin 1/2000 (AA6, Enzo Life Sciences, Farmingdale, NY), monoclonal Cdk5 1/500 (J-3, Santa Cruz Biotechnology, Dallas, TX), polyclonal p25/p35 1/500 (C-19, Santa Cruz Biotechnology), monoclonal ATM 1/1000 ([2C1 (1A1)]), (Abcam, Cambridge, United Kingdom), polyclonal ATM 1/2000 (phospho Ser1981[EP1890Y]) (Abcam), polyclonal Bax 1/1000 (D3R2M) (Cell signaling), monoclonal Bcl-2 1/500 (BD Biosciences, San Jose, CA), polyclonal β-actin 1/2500 (D6A8, Cell Signaling) and monoclonal GAPDH 1/2500 (Santa Cruz Biotechnology) in blocking buffer and then washed with TBS with 0.2% Tween-20. After washing, membranes were incubated with secondary antibodies in blocking buffer (IRDye 680 nm and 800 nm, 1/10 000, Li-Cor Biosciences) for 1 h, then washed again and quantified with the Odyssey Imaging System (Li-Cor Biosciences).

Immunofluorescence of FMRP and p-Ser^{1981}-ATM

Hippocampal neurons were fixed with 4% paraformaldehyde for 15 min and then permeabilized with 0.1% Triton X-100 for 10 min. Following blocking with 10% Normal Goat Serum (Life Technology) for 1 h, cells were incubated with either the monoclonal anti-FMRP antibody (1/200, Millipore) or the polyclonal anti-ATM antibody (phospho Ser1981[EP1890Y], 1/200, Abcam) and the polyclonal anti-MAP2b (1/500, Cell Signaling) overnight at 4 °C. After washing with PBS with 0.1% Tween-20, cells were incubated with goat anti-mouse Alexa 555 (1/500, Life technology) and goat anti-rabbit Oregon Green 488 (ThermoFisher Scientific), and with 2 drops per ml of NucBlue® Fixed Cell ReadyProbes® Reagent (Molecular Probes, Life Technology) for nuclei staining, all in 10% normal goat serum for 1 h at RT. The cells were washed and mounted in Prolong Gold antifade mounting medium and dried at RT for 48 hr, protected from light. Hippocampal neurons were then imaged using a Leica TCS SP8 STED 3X microscope in the super resolution mode for FMRP staining and using the resonant scanner for p-ATM labeled neurons in order to perform high speed scanning stack images through entire neurons. Images were then quantified using Fiji software (87) for FMRP staining and Bitplane Imaris (v.8.3, Bitplane AG, Zurich, Switzerland) for p-ATM stacks pictures.

Measurement of basal reactive oxygen species (ROS) level and production in live cell

After washing cells cultured in clear-bottom 96-well plates with PBS, they were incubated with 5 μM CellROX® Green (Life Technology) and NucBlue™ Live Cell Stain diluted in Locke's buffer (8.6 mM HEPES, 5.6 mM KCl, 154 mM NaCl, 5.6 mM glucose, 1.0 mM $MgCl_2$, 2.3 mM $CaCl_2$, and 0.1 μM glycine, pH 7.4) for 30 min at 37 °C. The cells were then washed 3 times and an additional 5 min incubation with 1,4-naphthoquinone (Acros Organics, Geel, Belgium) at 100 μM was used as a positive control while 200 μM N-acetylcysteine (NAC) (Sigma) was used as a negative control. Images of Wt and preCGG neurons were taken with a 20× objective in an automated high-throughput imager (ImageXpress Micro XLS; Molecular Devices, Sunnyvale, CA) under identical conditions.

For measurements of ROS production, cells were loaded as described above. Neurons loaded with CellROX® Green were transferred to a Fluorescence Laser Plate Reader (FLIPR, Molecular Devices) incubation chamber. FLIPR operates by illuminating the bottom of a 96-well microplate with LED light and measuring the fluorescence emissions with a cooled CCD camera in all 96 wells simultaneously, with the ability to add solutions with a 96-well robotic pipette while recording. The intracellular CellROX® Green was excited by 470–495 nm light, and emission in the 515–575 nm range was recorded during an exposure time of 0.4 s. After a 5-min baseline recording, 1,4-naphthoquinone or controls were added to wells at a 1:7 dilution. Fluorescence readings were taken every 2 s over a 15-min experimental time period. There were 5 wells of the same condition on each plate and the experiment was done in 5 repeats

Cytosolic Ca^{2+} imaging

At 14DIV, cultured hippocampal neurons were incubated with dye-loading buffer containing 4 μM Fluo-4 (Invitrogen) and 0.5 mg/ml BSA in Locke's (see above) for 30 min at 37 °C. After washing with Locke's buffer, the cells were excited at 488 nm and collected through a 515–575 nm (FITC) filter; the fluorescence signals were recorded at 33 frames/s using a charge-coupled device camera (model 512B; Photometrics, Tucson, AZ) under a 40× objective lens attached to an IX-71 inverted microscope (Olympus, Center Valley, PA) controlled by EasyRatioPro software (Photon Technologies International, Birmingham, NJ). Glu was added by pipetting 50μl of a 4X solution in each well containing 150μl of Locke's. The amplitude of fluorescence signals for each cell was presented as relative fluorescence changes (ΔF/F) after background subtraction. A fluorescence change (ΔF/F) exceeding 10% of baseline was considered a positive Ca^{2+} transient. The Ca^{2+} transient frequency and amplitude over a 10-min period were analyzed using Origin 8.5 software (OriginLab Corporation, Northampton, MA).

Cytosolic resting calcium measurement

Microelectrode recordings were performed as described previously (84). Briefly, resting $[Ca^{2+}]_i$ and resting plasma membrane potential (Vm) were recorded simultaneously using double-barreled Ca^{2+}-selective microelectrodes, prepared from 4-inch piggyback glass capillaries with outer/inner diameters of 1.51/0.75mm and 0.84/0.35mm (PB150F-4) (World Precision Instrument, Sarasota, FL). Capillaries were pulled to make short-taper microelectrodes with submicron diameter tip. The larger barrel, the "Ca^{2+} barrel", was silanized by exposure to dimethyldichlorosilane (Sigma) vapor. Twenty-four hours later, the tip was backfilled with calcium neutral liquid ion exchanger (IE200) (World Precision Instrument, Sarasota, FL) and the remainder of the barrel was backfilled with pCa7 solution 24 h later. The smaller barrel was backfilled with 3 mol/L KCl in order to measure V_m of the cells. Microelectrodes were calibrated before and after each experiment by recording the voltage response to Ca^{2+} solutions detected using a high impedance amplifier (Duo 773 Electrometer, World Precision Instruments). Only electrodes that produced a linear relationship between pCa 3 and pCa 7 with a Nernstian response (slope of ~29.5 mV per decade change in $[Ca^{2+}]$ at 25 °C) were used experimentally. Every impalement of the microelectrode in the soma of the neuron provided two simultaneous signals: a Ca^{2+} electrode potential (V_{CaE}) and V_m. The V_m potential was subtracted electronically from V_{CaE} potential, to produce a differential Ca^{2+}-specific potential (V_{Ca}, Fig. 4A) that represents the $[Ca^{2+}]_i$ concentration. V_m and V_{Ca} were filtered (30–50 kHz) to improve the signal-to-noise ratio. For some recordings, Tetrodotoxin (TTX) 1 μM (Tocris Bioscience, Bristol, United Kingdom) was added in the Lockes' buffer to silence the firing of the neurons. After one set of recordings, dantrolene 10 μM (Sigma) was added in the solution and incubated 10 min in the dark before starting a subsequent set of recordings.

μ-calpain activity assay

Calpain activity was measured using a calpain activity assay kit (Ab65308) (Abcam) according to the manufacturer's protocol. Briefly, cortical and hippocampal lysates were incubated with substrate (Ac-LLY-AFC, where AFC indicates 7-amino-4-trifluoromethyl coumarin) and 1x reaction buffer from the manufacturer for 1 h at 37 °C in the dark. Upon cleavage of substrate by calpain, the fluorogenic portion of AFC was detected at a wavelength of 505 nm following excitation at 400 nm. Fluorescence emission was measured using a SpectraMax MS Spectrofluorometer (Molecular Devices). Several concentrations of active calpain were used as a positive control and the addition of calpain inhibitor was used as a negative control. Each sample was measured in duplicate.

Statistical analysis

Graphing and statistical analyses were performed using GraphPad Prism software, Version 6.0, (GraphPad Software, Inc., San Diego, CA, USA). All values were expressed as mean ± SEM. Statistical significance between different groups was calculated using Student's *t*-test or by ANOVA followed by Tukey's multiple comparison test, as specified in each figure legend.

Supplementary Material

Supplementary Material is available at *HMG* online.

Acknowledgements

We thank Kelly Hiu-Ching Yuen for helping with the western blot; Yao Dong for assistance with animal mating and colony maintenance; Shane Antrobus with the genotyping; Drs. Kasia Koscielska, Jeanie Liu and Zhengyu Cao for developing the iPSC cell lines and advice on their culture.

Conflict of Interest statement. None declared.

Funding

National Institutes of Health [grants number R01 ES014901, P01 ES011269], IDDRC U54HD079125, DoD PR120921 and US EPA 83543201.

References

1. Hagerman, R.J., Leehey, M., Heinrichs, W., Tassone, F., Wilson, R., Hills, J., Grigsby, J., Gage, B. and Hagerman, P.J. (2001) Intention tremor, parkinsonism, and generalized brain atrophy in male carriers of fragile X. *Neurology*, **57**, 127–130.
2. Pfeiffer, B.E. and Huber, K.M. (2009) The state of synapses in fragile X syndrome. *Neuroscientist*, **15**, 549–567.
3. Hagerman, P.J. (2008) The fragile X prevalence paradox. *J. Med. Genet.*, **45**, 498–499.
4. Rodriguez-Revenga, L., Madrigal, I., Pagonabarraga, J., Xuncla, M., Badenas, C., Kulisevsky, J., Gomez, B. and Mila, M. (2009) Penetrance of FMR1 premutation associated pathologies in fragile X syndrome families. *Eur. J. Hum. Genet.*, **17**, 1359–1362.
5. Jacquemont, S., Hagerman, R.J., Leehey, M.A., Hall, D.A., Levine, R.A., Brunberg, J.A., Zhang, L., Jardini, T., Gane, L.W., Harris, S.W. *et al.* (2004) Penetrance of the fragile X-associated tremor/ataxia syndrome in a premutation carrier population. *JAMA*, **291**, 460–469.
6. Berry-Kravis, E., Abrams, L., Coffey, S.M., Hall, D.A., Greco, C., Gane, L.W., Grigsby, J., Bourgeois, J.A., Finucane, B., Jacquemont, S. *et al.* (2007) Fragile X-associated tremor/ataxia syndrome: clinical features, genetics, and testing guidelines. *Mov. Disord.*, **22**, 2018–2030. quiz 2140.
7. Aziz, M., Stathopulu, E., Callias, M., Taylor, C., Turk, J., Oostra, B., Willemsen, R. and Patton, M. (2003) Clinical features of boys with fragile X premutations and intermediate alleles. *Am. J. Med.Genet.*, **121B**, 119–127.
8. Hagerman, R. and Hagerman, P. (2013) Advances in clinical and molecular understanding of the FMR1 premutation and fragile X-associated tremor/ataxia syndrome. *Lancet Neurol.*, **12**, 786–798.
9. Cunningham, C.L., Martinez Cerdeno, V., Navarro Porras, E., Prakash, A.N., Angelastro, J.M., Willemsen, R., Hagerman, P.J., Pessah, I.N., Berman, R.F. and Noctor, S.C. (2011) Premutation CGG-repeat expansion of the Fmr1 gene impairs mouse neocortical development. *Hum. Mol. Genet.*, **20**, 64–79.
10. Chen, Y., Tassone, F., Berman, R.F., Hagerman, P.J., Hagerman, R.J., Willemsen, R. and Pessah, I.N. (2010) Murine hippocampal neurons expressing Fmr1 gene premutations show early developmental deficits and late degeneration. *Hum. Mol. Genet.*, **19**, 196–208.
11. Berman, R.F., Buijsen, R.A., Usdin, K., Pintado, E., Kooy, F., Pretto, D., Pessah, I.N., Nelson, D.L., Zalewski, Z., Charlet-Bergeurand, N. *et al.* (2014) Mouse models of the fragile X premutation and fragile X-associated tremor/ataxia syndrome. *J. Neurodev. Disord.*, **6**, 25.
12. Berman, R.F., Murray, K.D., Arque, G., Hunsaker, M.R. and Wenzel, H.J. (2012) Abnormal dendrite and spine morphology in primary visual cortex in the CGG knock-in mouse model of the fragile X premutation. *Epilepsia*, **53 Suppl 1**, 150–160.
13. Cao, Z., Hulsizer, S., Cui, Y., Pretto, D.L., Kim, K.H., Hagerman, P.J., Tassone, F. and Pessah, I.N. (2013) Enhanced asynchronous Ca(2+) oscillations associated with impaired glutamate transport in cortical astrocytes expressing Fmr1 gene premutation expansion. *J. Biol. Chem.*, **288**, 13831–13841.
14. Cao, Z., Hulsizer, S., Tassone, F., Tang, H.T., Hagerman, R.J., Rogawski, M.A., Hagerman, P.J. and Pessah, I.N. (2012) Clustered burst firing in FMR1 premutation hippocampal neurons: amelioration with allopregnanolone. *Hum. Mol. Genet.*, **21**, 2923–2935.
15. Iliff, A.J., Renoux, A.J., Krans, A., Usdin, K., Sutton, M.A. and Todd, P.K. (2013) Impaired activity-dependent FMRP translation and enhanced mGluR-dependent LTD in Fragile X premutation mice. *Hum. Mol. Genet.*, **22**, 1180–1192.
16. Pretto, D.I., Kumar, M., Cao, Z., Cunningham, C.L., Durbin-Johnson, B., Qi, L., Berman, R., Noctor, S.C., Hagerman, R.J., Pessah, I.N. *et al.* (2014) Reduced excitatory amino acid transporter 1 and metabotropic glutamate receptor 5 expression in the cerebellum of fragile X mental retardation gene 1 premutation carriers with fragile X-associated tremor/ataxia syndrome. *Neurobiol. Aging*, **35**, 1189–1197.
17. Liu, J., Koscielska, K.A., Cao, Z., Hulsizer, S., Grace, N., Mitchell, G., Nacey, C., Githinji, J., McGee, J., Garcia-Arocena, D. *et al.* (2012) Signaling defects in iPSC-derived fragile X premutation neurons. *Hum. Mol. Genet.*, **21**, 3795–3805.
18. Sellier, C., Usdin, K., Pastori, C., Peschansky, V.J., Tassone, F. and Charlet-Berguerand, N. (2014) The multiple molecular facets of fragile X-associated tremor/ataxia syndrome. *J. Neurodev. Disord.*, **6**, 23.
19. Willemsen, R., Hoogeveen-Westerveld, M., Reis, S., Holstege, J., Severijnen, L.A., Nieuwenhuizen, I.M., Schrier, M., van Unen, L., Tassone, F., Hoogeveen, A.T. *et al.* (2003) The FMR1 CGG repeat mouse displays ubiquitin-positive intranuclear neuronal inclusions; implications for the cerebellar tremor/ataxia syndrome. *Hum. Mol. Genet.*, **12**, 949–959.
20. Brouwer, J.R., Mientjes, E.J., Bakker, C.E., Nieuwenhuizen, I.M., Severijnen, L.A., Van der Linde, H.C., Nelson, D.L., Oostra, B.A. and Willemsen, R. (2007) Elevated Fmr1 mRNA levels and reduced protein expression in a mouse model with an unmethylated Fragile X full mutation. *Exp. Cell Res.*, **313**, 244–253.
21. Sellier, C., Rau, F., Liu, Y., Tassone, F., Hukema, R.K., Gattoni, R., Schneider, A., Richard, S., Willemsen, R., Elliott, D.J. *et al.* (2010) Sam68 sequestration and partial loss of function are associated with splicing alterations in FXTAS patients. *Embo J.*, **29**, 1248–1261.
22. Greco, C.M., Berman, R.F., Martin, R.M., Tassone, F., Schwartz, P.H., Chang, A., Trapp, B.D., Iwahashi, C., Brunberg, J., Grigsby, J. *et al.* (2006) Neuropathology of fragile X-associated tremor/ataxia syndrome (FXTAS). *Brain*, **129**, 243–255.
23. Greco, C.M., Hagerman, R.J., Tassone, F., Chudley, A.E., Del Bigio, M.R., Jacquemont, S., Leehey, M. and Hagerman, P.J. (2002) Neuronal intranuclear inclusions in a new cerebellar tremor/ataxia syndrome among fragile X carriers. *Brain*, **125**, 1760–1771.
24. Tassone, F., Iwahashi, C. and Hagerman, P.J. (2004) FMR1 RNA within the intranuclear inclusions of fragile X-associated tremor/ataxia syndrome (FXTAS). *RNA Biol.*, **1**, 103–105.
25. Wenzel, H.J., Hunsaker, M.R., Greco, C.M., Willemsen, R. and Berman, R.F. (2010) Ubiquitin-positive intranuclear inclusions in neuronal and glial cells in a mouse model of the fragile X premutation. *Brain Res.*, **1318**, 155–166.
26. Iwahashi, C.K., Yasui, D.H., An, H.J., Greco, C.M., Tassone, F., Nannen, K., Babineau, B., Lebrilla, C.B., Hagerman, R.J. and

Hagerman, P.J. (2006) Protein composition of the intranuclear inclusions of FXTAS. *Brain*, **129**, 256–271.
27. Hoem, G., Raske, C.R., Garcia-Arocena, D., Tassone, F., Sanchez, E., Ludwig, A.L., Iwahashi, C.K., Kumar, M., Yang, J.E. and Hagerman, P.J. (2011) CGG-repeat length threshold for FMR1 RNA pathogenesis in a cellular model for FXTAS. *Hum. Mol. Genet.*, **20**, 2161–2170.
28. Todd, P.K., Oh, S.Y., Krans, A., He, F., Sellier, C., Frazer, M., Renoux, A.J., Chen, K.C., Scaglione, K.M., Basrur, V. *et al.* (2013) CGG repeat-associated translation mediates neurodegeneration in fragile X tremor ataxia syndrome. *Neuron*, **78**, 440–455.
29. Oh, S.Y., He, F., Krans, A., Frazer, M., Taylor, J.P., Paulson, H.L. and Todd, P.K. (2015) RAN translation at CGG repeats induces ubiquitin proteasome system impairment in models of fragile X-associated tremor ataxia syndrome. *Hum. Mol. Genet.*, **24**, 4317–4326.
30. Kearse, M.G. and Todd, P.K. (2014) Repeat-associated non-AUG translation and its impact in neurodegenerative disease. *Neurotherapeutics*, **11**, 721–731.
31. Sellier, C., Buijsen, R.A., He, F., Natla, S., Jung, L., Tropel, P., Gaucherot, A., Jacobs, H., Meziane, H., Vincent, A. *et al.* (2017) Translation of expanded CGG repeats into FMRpolyG is pathogenic and may contribute to fragile X tremor ataxia syndrome. *Neuron*, **93**, 331–347.
32. Kawauchi, T. (2014) Cdk5 regulates multiple cellular events in neural development, function and disease. *Dev. Growth Differ.*, **56**, 335–348.
33. Patrick, G.N., Zukerberg, L., Nikolic, M., de la Monte, S., Dikkes, P. and Tsai, L.H. (1999) Conversion of p35 to p25 deregulates Cdk5 activity and promotes neurodegeneration. *Nature*, **402**, 615–622.
34. Tian, B., Yang, Q. and Mao, Z. (2009) Phosphorylation of ATM by Cdk5 mediates DNA damage signalling and regulates neuronal death. *Nat. Cell Biol.*, **11**, 211–218.
35. Yu, H.P., Xie, J.M., Li, B., Sun, Y.H., Gao, Q.G., Ding, Z.H., Wu, H.R. and Qin, Z.H. (2015) TIGAR regulates DNA damage and repair through pentosephosphate pathway and Cdk5-ATM pathway. *Sci. Rep.*, **5**, 9853.
36. Wu, J., Zhang, X., Yan, Y., Tang, Z., Sun, X., Huo, G. and Liao, Z. (2016) The Crucial Role of Cyclin-Dependent Kinase-5-Ataxia-Telangiectasia Mutated Axis in ICH-Induced Neuronal Injury of Rat Model. *Mol. Neurobiol.*, **53**, 6301–6308.
37. Kastan, M.B. and Lim, D.S. (2000) The many substrates and functions of ATM. *Nat. Rev. Mol. Cell Biol.*, **1**, 179–186.
38. Li, J., Han, Y.R., Plummer, M.R. and Herrup, K. (2009) Cytoplasmic ATM in neurons modulates synaptic function. *Curr. Biol.*, **19**, 2091–2096.
39. Shiloh, Y. and Ziv, Y. (2013) The ATM protein kinase: regulating the cellular response to genotoxic stress, and more. *Nat. Rev. Mol. Cell Biol.*, **14**, 197–210.
40. Bear, M.F., Huber, K.M. and Warren, S.T. (2004) The mGluR theory of fragile X mental retardation. *Trends Neurosci.*, **27**, 370–377.
41. Schmunk, G., Boubion, B.J., Smith, I.F., Parker, I. and Gargus, J.J. (2015) Shared functional defect in IP(3)R-mediated calcium signaling in diverse monogenic autism syndromes. *Transl Psychiatry*, **5**, e643.
42. Clause, A., Kim, G., Sonntag, M., Weisz, C.J., Vetter, D.E., Rubsamen, R. and Kandler, K. (2014) The precise temporal pattern of prehearing spontaneous activity is necessary for tonotopic map refinement. *Neuron*, **82**, 822–835.
43. Paula-Lima, A.C., Adasme, T. and Hidalgo, C. (2014) Contribution of Ca2+ release channels to hippocampal synaptic plasticity and spatial memory: potential redox modulation. *Antioxid. Redox Signal*, **21**, 892–914.
44. Yan, X.X., Jeromin, A. and Jeromin, A. (2012) Spectrin Breakdown Products (SBDPs) as Potential Biomarkers for Neurodegenerative Diseases. *Curr. Transl Geriatr. Exp. Gerontol. Rep.*, **1**, 85–93.
45. Lee, M.S., Kwon, Y.T., Li, M., Peng, J., Friedlander, R.M. and Tsai, L.H. (2000) Neurotoxicity induces cleavage of p35 to p25 by calpain. *Nature*, **405**, 360–364.
46. Xiang, H., Kinoshita, Y., Knudson, C.M., Korsmeyer, S.J., Schwartzkroin, P.A. and Morrison, R.S. (1998) Bax involvement in p53-mediated neuronal cell death. *J. Neurosci.*, **18**, 1363–1373.
47. Berridge, M.J. (2016) Vitamin D, reactive oxygen species and calcium signalling in ageing and disease. *Philos. Trans. R. Soc. Lond. B Biol. Sci.*, **371**, pii: 20150434.
48. Roberts, R.A., Laskin, D.L., Smith, C.V., Robertson, F.M., Allen, E.M., Doorn, J.A. and Slikker, W. (2009) Nitrative and oxidative stress in toxicology and disease. *Toxicol. Sci.*, **112**, 4–16.
49. Thor, H., Smith, M.T., Hartzell, P., Bellomo, G., Jewell, S.A. and Orrenius, S. (1982) The metabolism of menadione (2-methyl-1,4-naphthoquinone) by isolated hepatocytes. A study of the implications of oxidative stress in intact cells. *J. Biol. Chem.*, **257**, 12419–12425.
50. Uhlen, P., Fritz, N., Smedler, E., Malmersjo, S. and Kanatani, S. (2015) Calcium signaling in neocortical development. *Dev. Neurobiol.*, **75**, 360–368.
51. Kaplan, E.S., Cao, Z., Hulsizer, S., Tassone, F., Berman, R.F., Hagerman, P.J. and Pessah, I.N. (2012) Early mitochondrial abnormalities in hippocampal neurons cultured from Fmr1 pre-mutation mouse model. *J. Neurochem.*, **123**, 613–621.
52. Brouwer, J.R., Huizer, K., Severijnen, L.A., Hukema, R.K., Berman, R.F., Oostra, B.A. and Willemsen, R. (2008) CGG-repeat length and neuropathological and molecular correlates in a mouse model for fragile X-associated tremor/ataxia syndrome. *J. Neurochem.*, **107**, 1671–1682.
53. Brouwer, J.R., Severijnen, E., de Jong, F.H., Hessl, D., Hagerman, R.J., Oostra, B.A. and Willemsen, R. (2008) Altered hypothalamus-pituitary-adrenal gland axis regulation in the expanded CGG-repeat mouse model for fragile X-associated tremor/ataxia syndrome. *Psychoneuroendocrinology*, **33**, 863–873.
54. Tassone, F., Hagerman, R.J., Taylor, A.K., Gane, L.W., Godfrey, T.E. and Hagerman, P.J. (2000) Elevated levels of FMR1 mRNA in carrier males: a new mechanism of involvement in the fragile-X syndrome. *Am. J. Hum. Genet.*, **66**, 6–15.
55. Arocena, D.G., Iwahashi, C.K., Won, N., Beilina, A., Ludwig, A.L., Tassone, F., Schwartz, P.H. and Hagerman, P.J. (2005) Induction of inclusion formation and disruption of lamin A/C structure by premutation CGG-repeat RNA in human cultured neural cells. *Hum. Mol. Genet.*, **14**, 3661–3671.
56. Mattson, M.P. (2007) Calcium and neurodegeneration. *Aging Cell*, **6**, 337–350.
57. Huang, G.Z. and Woolley, C.S. (2012) Estradiol acutely suppresses inhibition in the hippocampus through a sex-specific endocannabinoid and mGluR-dependent mechanism. *Neuron*, **74**, 801–808.
58. Fester, L., Brandt, N., Windhorst, S., Prols, F., Blaute, C. and Rune, G.M. (2016) Control of aromatase in hippocampal neurons. *J. Steroid Biochem. Mol. Biol.*, **160**, 9–14.
59. Paul-Pletzer, K., Yamamoto, T., Bhat, M.B., Ma, J., Ikemoto, N., Jimenez, L.S., Morimoto, H., Williams, P.G. and Parness, J. (2002) Identification of a dantrolene-binding sequence on

the skeletal muscle ryanodine receptor. *J. Biol. Chem.*, **277**, 34918–34923.
60. Inan, S. and Wei, H. (2010) The cytoprotective effects of dantrolene: a ryanodine receptor antagonist. *Anesth. Analg.*, **111**, 1400–1410.
61. Chen, X., Wu, J., Lvovskaya, S., Herndon, E., Supnet, C. and Bezprozvanny, I. (2011) Dantrolene is neuroprotective in Huntington's disease transgenic mouse model. *Mol. Neurodegener.*, **6**, 81.
62. Mody, I. and MacDonald, J.F. (1995) NMDA receptor-dependent excitotoxicity: the role of intracellular Ca2+ release. *Trends Pharmacol. Sci.*, **16**, 356–359.
63. Wei, H. and Perry, D.C. (1996) Dantrolene is cytoprotective in two models of neuronal cell death. *J. Neurochem.*, **67**, 2390–2398.
64. Bassell, G.J. and Warren, S.T. (2008) Fragile X syndrome: loss of local mRNA regulation alters synaptic development and function. *Neuron*, **60**, 201–214.
65. Guo, W., Ceolin, L., Collins, K.A., Perroy, J. and Huber, K.M. (2015) Elevated CaMKIIalpha and Hyperphosphorylation of Homer Mediate Circuit Dysfunction in a Fragile X Syndrome Mouse Model. *Cell Rep.*, **13**, 2297–2311.
66. Contractor, A., Klyachko, V.A. and Portera-Cailliau, C. (2015) Altered Neuronal and Circuit Excitability in Fragile X Syndrome. *Neuron*, **87**, 699–715.
67. Sidorov, M.S., Auerbach, B.D. and Bear, M.F. (2013) Fragile X mental retardation protein and synaptic plasticity. *Mol. Brain*, **6**, 15.
68. Muddashetty, R.S., Kelic, S., Gross, C., Xu, M. and Bassell, G.J. (2007) Dysregulated metabotropic glutamate receptor-dependent translation of AMPA receptor and postsynaptic density-95 mRNAs at synapses in a mouse model of fragile X syndrome. *J. Neurosci.*, **27**, 5338–5348.
69. Burguete, A.S., Almeida, S., Gao, F.B., Kalb, R., Akins, M.R. and Bonini, N.M. (2015) GGGGCC microsatellite RNA is neuritically localized, induces branching defects, and perturbs transport granule function. *Elife*, **4**, e08881.
70. Loomis, E.W., Sanz, L.A., Chedin, F. and Hagerman, P.J. (2014) Transcription-associated R-loop formation across the human FMR1 CGG-repeat region. *PLoS Genet.*, **10**, e1004294.
71. Jin, P., Zarnescu, D.C., Zhang, F., Pearson, C.E., Lucchesi, J.C., Moses, K. and Warren, S.T. (2003) RNA-mediated neurodegeneration caused by the fragile X premutation rCGG repeats in Drosophila. *Neuron*, **39**, 739–747.
72. Nixon, R.A., Saito, K.I., Grynspan, F., Griffin, W.R., Katayama, S., Honda, T., Mohan, P.S., Shea, T.B. and Beermann, M. (1994) Calcium-activated neutral proteinase (calpain) system in aging and Alzheimer's disease. *Ann. New York Acad. Sci.*, **747**, 77–91.
73. Smith, P.D., Crocker, S.J., Jackson-Lewis, V., Jordan-Sciutto, K.L., Hayley, S., Mount, M.P., O'Hare, M.J., Callaghan, S., Slack, R.S., Przedborski, S. *et al.* (2003) Cyclin-dependent kinase 5 is a mediator of dopaminergic neuron loss in a mouse model of Parkinson's disease. *Proc. Natl Acad. Sci. U.S.A.*, **100**, 13650–13655.
74. Gafni, J. and Ellerby, L.M. (2002) Calpain activation in Huntington's disease. *J. Neurosci.*, **22**, 4842–4849.
75. Roy, D. and Lieber, M.R. (2009) G clustering is important for the initiation of transcription-induced R-loops in vitro, whereas high G density without clustering is sufficient thereafter. *Mol. Cell Biol.*, **29**, 3124–3133.
76. Guo, Z., Kozlov, S., Lavin, M.F., Person, M.D. and Paull, T.T. (2010) ATM activation by oxidative stress. *Science*, **330**, 517–521.
77. Siddoway, B., Hou, H., Yang, H., Petralia, R. and Xia, H. (2014) Synaptic activity bidirectionally regulates a novel sequence-specific S-Q phosphoproteome in neurons. *J. Neurochem.*, **128**, 841–851.
78. Schelman, W.R., Andres, R.D., Sipe, K.J., Kang, E. and Weyhenmeyer, J.A. (2004) Glutamate mediates cell death and increases the Bax to Bcl-2 ratio in a differentiated neuronal cell line. *Brain Res. Mol. Brain Res.*, **128**, 160–169.
79. Napoli, E., Song, G., Schneider, A., Hagerman, R., Eldeeb, M.A., Azarang, A., Tassone, F. and Giulivi, C. (2016) Warburg effect linked to cognitive-executive deficits in FMR1 premutation. *Faseb J.*, **30**, 3334–3351.
80. Napoli, E., Song, G., Wong, S., Hagerman, R. and Giulivi, C. (2016) Altered Bioenergetics in Primary Dermal Fibroblasts from Adult Carriers of the FMR1 Premutation Before the Onset of the Neurodegenerative Disease Fragile X-Associated Tremor/Ataxia Syndrome. *Cerebellum*, **15**, 552–564.
81. Ross-Inta, C., Omanska-Klusek, A., Wong, S., Barrow, C., Garcia-Arocena, D., Iwahashi, C., Berry-Kravis, E., Hagerman, R.J., Hagerman, P.J. and Giulivi, C. (2010) Evidence of mitochondrial dysfunction in fragile X-associated tremor/ataxia syndrome. *Biochem. J.*, **429**, 545–552.
82. Dafinca, R., Scaber, J., Ababneh, N., Lalic, T., Weir, G., Christian, H., Vowles, J., Douglas, A.G., Fletcher-Jones, A., Browne, C. *et al.* (2016) C9orf72 hexanucleotide expansions are associated with altered endoplasmic reticulum calcium homeostasis and stress granule formation in induced pluripotent stem cell-derived neurons from patients with amyotrophic lateral sclerosis and frontotemporal dementia. *Stem Cells*, **34**, 2063–2078.
83. Cleary, J.D. and Ranum, L.P. (2013) Repeat-associated non-ATG (RAN) translation in neurological disease. *Hum. Mol. Genet.*, **22**, R45–R51.
84. Lopez, J.R., Lyckman, A., Oddo, S., Laferla, F.M., Querfurth, H.W. and Shtifman, A. (2008) Increased intraneuronal resting [Ca2+] in adult Alzheimer's disease mice. *J. Neurochem.*, **105**, 262–271.
85. Hodgson, J.G., Agopyan, N., Gutekunst, C.A., Leavitt, B.R., LePiane, F., Singaraja, R., Smith, D.J., Bissada, N., McCutcheon, K., Nasir, J. *et al.* (1999) A YAC mouse model for Huntington's disease with full-length mutant huntingtin, cytoplasmic toxicity, and selective striatal neurodegeneration. *Neuron*, **23**, 181–192.
86. Lopez, J.R., Kolster, J., Uryash, A., Esteve, E., Altamirano, F. and Adams, J.A. (2016) Dysregulation of intracellular Ca2+ in dystrophic cortical and hippocampal neurons. *Mol. Neurobiol.*, DOI:10.1007/s12035-016-0311-7.
87. Schindelin, J., Arganda-Carreras, I., Frise, E., Kaynig, V., Longair, M., Pietzsch, T., Preibisch, S., Rueden, C., Saalfeld, S., Schmid, B. *et al.* (2012) Fiji: an open-source platform for biological-image analysis. *Nat. Methods*, **9**, 676–682.
88. D'Hulst, C., Heulens, I., Brouwer, J.R., Willemsen, R., De Geest, N., Reeve, S.P., De Deyn, P.P., Hassan, B.A. and Kooy, R.F. (2009) Expression of the GABAergic system in animal models for fragile X syndrome and fragile X associated tremor/ataxia syndrome (FXTAS). *Brain Res.*, **1253**, 176–183.
89. Hunsaker, M.R., Goodrich-Hunsaker, N.J., Willemsen, R. and Berman, R.F. (2010) Temporal ordering deficits in female CGG KI mice heterozygous for the fragile X premutation. *Behav. Brain Res.*, **213**, 263–268.
90. Hunsaker, M.R., Greco, C.M., Spath, M.A., Smits, A.P., Navarro, C.S., Tassone, F., Kros, J.M., Severijnen, L.A., Berry-Kravis, E.M., Berman, R.F. *et al.* (2011) Widespread non-central

nervous system organ pathology in fragile X premutation carriers with fragile X-associated tremor/ataxia syndrome and CGG knock-in mice. *Acta Neuropathol.*, **122**, 467–479.
91. Hunsaker, M.R., Kim, K., Willemsen, R. and Berman, R.F. (2012) CGG trinucleotide repeat length modulates neural plasticity and spatiotemporal processing in a mouse model of the fragile X premutation. *Hippocampus*, **22**, 2260–2275.
92. Hunsaker, M.R., von Leden, R.E., Ta, B.T., Goodrich-Hunsaker, N.J., Arque, G., Kim, K., Willemsen, R. and Berman, R.F. (2011) Motor deficits on a ladder rung task in male and female adolescent and adult CGG knock-in mice. *Behav. Brain Res.*, **222**, 117–121.
93. Hunsaker, M.R., Wenzel, H.J., Willemsen, R. and Berman, R.F. (2009) Progressive spatial processing deficits in a mouse model of the fragile X premutation. *Behav. Neurosci.*, **123**, 1315–1324.
94. Napoli, E., Ross-Inta, C., Song, G., Wong, S., Hagerman, R., Gane, L.W., Smilowitz, J.T., Tassone, F. and Giulivi, C. (2016) Premutation in the Fragile X Mental Retardation 1 (FMR1) Gene Affects Maternal Zn-milk and Perinatal Brain Bioenergetics and Scaffolding. *Front. Neurosci.*, **10**, 159.
95. Renoux, A.J., Sala-Hamrick, K.J., Carducci, N.M., Frazer, M., Halsey, K.E., Sutton, M.A., Dolan, D.F., Murphy, G.G. and Todd, P.K. (2014) Impaired sensorimotor gating in Fmr1 knock out and Fragile X premutation model mice. *Behav. Brain Res.*, **267**, 42–45.
96. Schluter, E.W., Hunsaker, M.R., Greco, C.M., Willemsen, R. and Berman, R.F. (2012) Distribution and frequency of intranuclear inclusions in female CGG KI mice modeling the fragile X premutation. *Brain Res.*, **1472**, 124–137.
97. Van Dam, D., Errijgers, V., Kooy, R.F., Willemsen, R., Mientjes, E., Oostra, B.A. and De Deyn, P.P. (2005) Cognitive decline, neuromotor and behavioural disturbances in a mouse model for fragile-X-associated tremor/ataxia syndrome (FXTAS). *Behav. Brain Res.*, **162**, 233–239.